SKI Report 02:28

Research

Evaluation of the SCANAIR Computer Code

Lars Olof Jernkvist
Ali Massih

November 2001

ISSN 1104–1374
ISRN SKI-R-02/28-SE

SKI PERSPECTIVE

How this project has contributed to SKI:s research goals

The overall goals for SKI rearch are:

- to give a basis for SKI:s supervision
- to maintain and develop the competence and research capacity within areas which are important to reactor safety
- to contribute directly to the Swedish safety work.

This project has mainly contributed to the strategic goal of giving a basis for SKI:s supervision by means of an independent evaluation of the computer code SCANAIR with respect to its applicability for licensing purposes. The project has also contributed to the goal of maintaining and developing the competence and research capacity within Sweden. SCANAIR was developed by IRSN and was obtained through SKI:s participation in the OECD/NEA CABRI Water Loop Project.

The results from the limited study of SCANAIR has mainly been positive, the report especially emphasizes the unique pellet material model. The report however indicates that some of the models used should be improved; clad material model and heat transfer models clad – water. The conclusion is that SCANAIR is an adequate computer code for predicting thermal-mechanical behavior of a fuel rod during a postulated RIA although the code would benefit from further calibration to experimental data.

Project information:
Project manager: *Ingrid Töcksberg, Department of Reactor Technology, SKI*
Project number: *14.6-010185/01088*

SKI Report 02:28

Research

Evaluation of the SCANAIR Computer Code

Lars Olof Jernkvist
Ali Massih

Quantum Technologies AB
Uppsala Science Park
SE-751 83 Uppsala
Sweden

November 2001

SKI Project Number 01088

List of contents

Summary

The SCANAIR computer code, version 3.2, has been evaluated from the standpoint of its capability to analyze, simulate and predict nuclear fuel behavior during severe power transients. SCANAIR calculates the thermal and mechanical behavior of a pressurized water reactor (PWR) fuel rod during a postulated reactivity initiated accident (RIA), and our evaluation indicates that SCANAIR is a state of the art computational tool for this purpose.

Our evaluation starts by reviewing the basic theoretical models in SCANAIR, namely the governing equations for heat transfer, the mechanical response of fuel and clad, and the fission gas release behavior. The numerical methods used to solve the governing equations are briefly reviewed, and the range of applicability of the models and their limitations are discussed and illustrated with examples.

Next, the main features of the SCANAIR user interface are delineated. The code requires an extensive amount of input data, in order to define burnup-dependent initial conditions to the simulated RIA. These data must be provided in a special format by a thermal-mechanical fuel rod analysis code. The user also has to supply the transient power history under RIA as input, which requires a code for neutronics calculation.

The programming structure and documentation of the code are also addressed in our evaluation. SCANAIR is programmed in Fortran-77, and makes use of several general Fortran-77 libraries for handling input/output, data storage and graphical presentation of computed results. The documentation of SCANAIR and its helping libraries is generally of good quality. A drawback with SCANAIR in its present form, is that the code and its pre- and post-processors are tied to computers running the Unix or Linux operating systems.

As part of our evaluation, we have performed a large number of computations with SCANAIR, some of which are documented in this report. The computations presented here include a hypothetical RIA in a high-burnup fuel rod. This test case is used to check the validity of SCANAIR installation in a new computer environment, but also to examine the output response of the code to an RIA-type load. Moreover, we have used independent computational methods to verify and compare some of the SCANAIR results for this reference case. The outcome is encouraging.

In addition, we have attempted to simulate with SCANAIR a ramp test performed at the Studsvik R2 reactor, and a rod in the Studsvik TRANSRAMP-IV project was selected for this purpose. Although SCANAIR is not designed to simulate “moderate” transients like the one considered here, we have found the results on fission gas release and clad plastic strain in fair agreement with measured data.

Finally, we have performed computations on an existent RIA test made on a pre-irradiated rod in the CABRI reactor, to wit the REP-Na2 rod in the REP-Na test series. Rod Na2 was subjected to a fast RIA-type pulse with a pulse-width of 0.9 ms and a peak linear power density of about 40 MW/m. Also for this test case, SCANAIR exhibited good performance with reasonable execution times on personal computers with the Linux operating system.

We have not subjected SCANAIR to extensive testing and benchmarking against experimental data, nor to a wide-range of parametric studies to locate possible faults of the code in analyses of highly irradiated fuel rods under RIA. However, our evaluation and testing indicate that the models used for pellet and clad (visco)plastic deformation and axial mixing of released fission products should be improved. Nevertheless, our limited study with SCANAIR has been positive. Although it would benefit from further calibration to experimental data, we believe that SCANAIR is an adequate computer code for predicting thermal-mechanical behavior of a fuel rod during a postulated RIA.

Sammanfattning

Datorprogrammet SCANAIR, version 3.2, har utvärderats med utgångspunkt från programmets förmåga att analysera, simulera och prediktera beteendet hos kärnbränsle under kraftiga effekttransienter. SCANAIR beräknar det termiska och mekaniska beteendet hos en kärnbränslestav i en tryckvattenreaktor (PWR) under en postulerad reaktivitetstransient (RIA), och vår utvärdering visar att SCANAIR är ett framstående beräkningsverktyg för detta ändamål.

Vår utvärdering börjar med en genomgång av de grundläggande teoretiska modellerna i SCANAIR, nämligen de styrande ekvationerna för värmetransport, mekaniskt beteende hos bränslekuts och kapsling, samt frigörelse av gasformiga fissionsprodukter. De numeriska metoder som används för att lösa dessa ekvationer berörs, och modellernas tillämplighet och begränsningar diskuteras och belyses med exempel.

De viktigaste dragen hos SCANAIRS användargränssnitt beskrives härnäst. Programmet behöver en stor mängd indata, som används för att definiera det utbränningsberoende begynnelsetillståndet till den simulerade reaktivitetstransienten. Dessa indata måste överföras i ett speciellt format från ett beräkningsprogram för termomekanisk bränslestavanalys. Användaren måste dessutom föreskriva effekthistorien under RIA, vilket förutsätter ett program för reaktorfysikberäkningar.

Även programkodens struktur och dokumentation belyses i vår utvärdering. SCANAIR är programmerat i Fortran-77, och använder ett flertal generella bibliotek skrivna i detta språk för att hantera in/utdata, datalagring och grafisk presentation av resultat. Dokumentationen av SCANAIR och dess bibliotek är i stort av god kvalitet. En nackdel är att SCANAIR och dess pre- och post-processorer i nuvarande form är bundna till datorer med operativsystemet Unix eller Linux.

Ett stort antal beräkningar med SCANAIR har utförts som en del av vår utvärdering, och resultat från några av dessa beräkningar presenteras i rapporten. Till dessa hör en beräkning av en hypotetisk RIA i en högutbränd bränslestav. Detta testfall används för att verifiera installeringen av SCANAIR i en ny datormiljö, men även för att studera programmets respons med avseende på ett RIA-liknande belastningsfall. Vi har dessutom använt oberoende beräkningsmetoder för att verifiera SCANAIRS beräkningsresultat för detta referensfall. Resultaten är positiva.

Vi har även försökt använda SCANAIR för att simulera ett ramptest utfört i R2-rektorn i Studsvik, och en bränslestav från Studsvikprojektet TRANSRAMP-IV valdes för denna simulering. Trots att SCANAIR egentligen ej är avsett för simulering av ”milda” transienter som denna, så har vi funnit att beräknad fissionsgasfrigörelse och plastisk kapslingstöjning stämmer relativt väl med mätdata.

Slutligen har vi genomfört beräkningar av ett befintligt RIA-prov, vilket utförts på en bestrålad bränslestav i CABRI-reaktorn, nämligen stav REP-Na2 i provserien REP-Na. Denna stav utsattes för en RIA-liknande effektpuls med en pulsvidd om 0.9 ms och en maximal längdvärmebelastning om 40 MW/m. SCANAIR fungerade väl även för detta fall, och gav rimliga exekveringstider på Linuxbaserade persondatorer.

Vi har i detta arbete ej genomfört någon omfattande provning eller verifiering av SCANAIR, ej heller någon heltäckande parameterstudie för att lokalisera eventuella svagheter vid analyser av högutbrända bränslestavar under RIA. Vår utvärdering och provning visar dock att modellerna för kutsens och kapslingens (visko)plastiska deformation samt modellen för axiell blandning av frigjorda fissionsprodukter bör förbättras. Detta oaktat, så har vår begränsade utvärdering av SCANAIR givit positiva resultat. Även om programmet skulle gagnas av ytterligare kalibrering gentemot experimentella data, så anser vi att SCANAIR är ett fullgott beräkningsprogram för att prediktera bränslestavens termomekaniska beteende under postulerade reaktivitetstransienter.

1 Introduction

The purpose of this report is to document an evaluation made of the computer program SCANAIR. The SCANAIR code is designed to simulate the thermal-mechanical behavior of a pressurized water reactor (PWR) fuel rod during a reactivity insertion accident (RIA). A reactivity insertion accident in fission-reactors is characterized by a rapid reactivity increase in the nuclear fuel, caused by breakdown of the reactor control system, which in turn leads to a fast power excursion up to extremely high power levels. In light water reactors (LWRs), the peak power level during RIA will be governed by the reactivity of the ejected control rod (rod worth), the Doppler coefficient, fuel power peaking factor and fraction of delayed neutrons.

The SCANAIR code is developed by the *Institut de Protection et de Sûreté Nucléaire* (IPSN) in collaboration with *Electricité de France* (EDF) within the frames of the CABRI-REP-Na program. SCANAIR consists of three basic modules, responsible for calculation of thermal dynamics, structural mechanics and fission gas behavior. The code is one-dimensional in makeup, *i.e*. it solves all fundamental equations for heat transfer, deformations and fission gas release with respect to the fuel rod radial direction, but takes into account each axial segment of the rod separately.

The computational flow between the three modules in SCANAIR is schematically illustrated in figure 1. The computations involve the following exchange of data between the three modules:

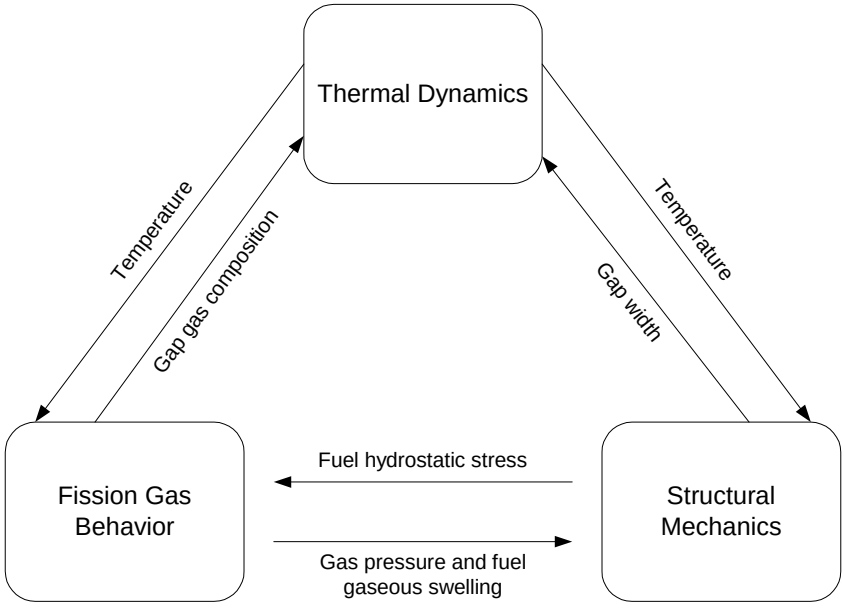

Figure 1: SCANAIR computational scheme.

- **Thermal Dynamics → Structural Mechanics**:
  Fuel and clad temperatures are transferred from the Thermal Dynamics module to the Structural Mechanics module for calculation of thermal expansion and temperature dependent mechanical properties of the material.
- **Thermal Dynamics → Fission Gas Behavior**:
  Temperature data are transferred to the Fission Gas Behavior module for calculation of gas diffusion coefficients, gas bubble swelling, etc.
- **Structural Mechanics → Thermal Dynamics**:
  The pellet-clad gap width data are transferred from the Structural Mechanics to the Thermal Dynamics module.
- **Structural Mechanics → Fission Gas Behavior**
  The fuel hydrostatic stress is needed in calculations of fuel fission gas swelling.
- **Fission Gas Behavior → Structural Mechanics**:
  Fuel gaseous swelling and rod internal pressure data are transferred from the Fission Gas Behavior to the Structural Mechanics module.
- **Fission Gas Behavior → Thermal Dynamics**:
  Fission gas release reduces the gap thermal conductance, thus increasing fuel temperature. Gas composition data are therefore transferred to the Thermal Dynamics module.

It should be noted, that the SCANAIR code does not include a neutronic module for generating the loads (power excursion) imparted to the fuel during an RIA. Neither does it comprise steady-state models for calculation of the fuel behavior prior to the accident. These data must therefore be supplied by other external codes, and need to be inputted to SCANAIR in special formats.

According to Federici *et al*. (2000a), the SCANAIR code has been benchmarked against measured data obtained from the CABRI test reactor program, Papin *et al*. (1996) and Frizonnet *et al*. (1997), as well as data from NSRR, Fuketa *et al*. (1997). Individual models in SCANAIR have also been compared and verified with several separate effect studies, Lemoine and Balourdet (1997). For example, clad mechanical properties have been verified within the PROMETRA program, Balourdet *et al*. (1999). The clad-to-coolant heat transfer calculations during fast power excursions have been verified within the PATRICIA program and the transient fission gas release within the RIA-SILENE program. Moreover, the numerics of the code have been validated either against analytical solutions or against a more detailed finite element code, CASTEM, Constantinescu *et al*. (1998)

The organization of this report is as follows: In chapter 2, we briefly review the SCANAIR models, namely the basic equations used and assumptions made in thermal analysis, structural analysis and fission gas behavior. Chapter 3 presents an overview of the SCANAIR interface, *i.e*., the input and output of the code. In chapter 4, we provide some remarks on the programming aspects of SCANAIR. The results of our computations with SCANAIR are finally presented in chapter 5. In that chapter, we present the computations made on a test case used for verification of the installation and compilation of the code in our system. This case is a hypothetical RIA-like transient, postulated to occur on a high burnup PWR fuel rod. This test case has also been analyzed by use of the STRUCTUS code, for the purpose of independent model verification. In addition, the SCANAIR code has been used to simulate a ramp test made on a PWR rod (TRANSRAMP-IV) at Studsvik, and a realistic RIA simulation test performed in the CABRI test reactor. The outcome of these computations is also presented in chapter 5.

2 SCANAIR models

The SCANAIR code is designed to simulate fuel thermal-mechanical behavior during a postulated RIA. As in many steady-state fuel behavior codes, the modeling comprises three main components, Lemare and Latché (1995):

1. Thermal analysis for calculation of fuel and clad temperatures, including calculation of heat transfer across the pellet-clad gap and from the clad to the coolant.
2. Structural analysis for computation of deformations and stresses.
3. Calculation of fuel fission gas release.

All the SCANAIR models are designed to treat the conditions that prevail during an RIA, *i.e*. applications to other reactor transients are unwarranted.

2.1 Thermal analysis

In the thermal analysis, the fuel rod and coolant channel geometry where heat transfer takes place is schematically shown in figure 2. Heat transfer takes place in the fuel, the clad tube, the fuel pellet-clad gap, the coolant and the shroud (in case of experiment simulations). Only radial heat transfer is modeled. In SCANAIR, three types of heat transfer are considered: *i*) heat conduction through solids, *i.e*. in fuel, clad and shroud, *ii*) gas gap conductance, *iii*) heat transfer into and along the coolant channel.

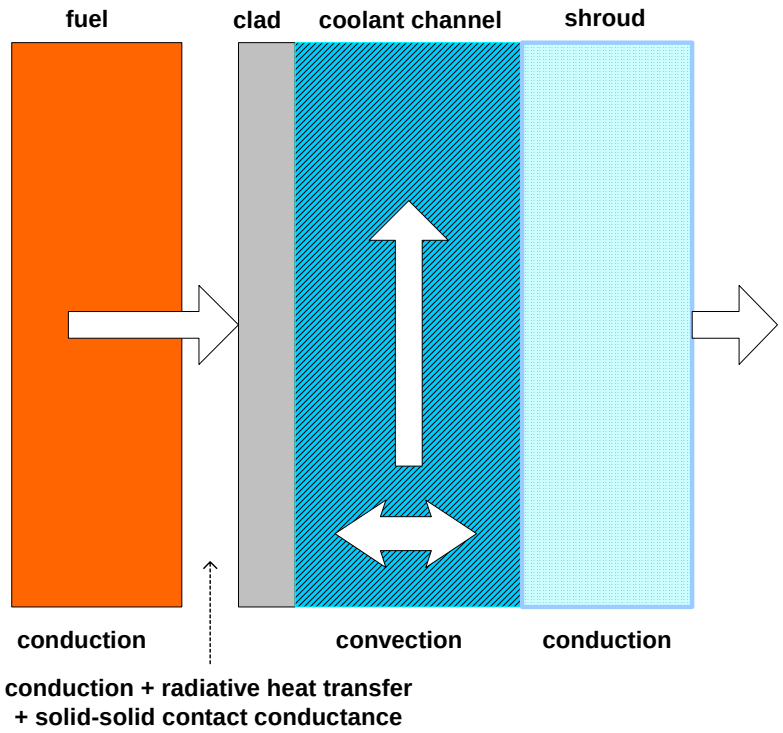

Figure 2: Heat transfer modeled in SCANAIR.

2.1.1 Fuel, clad and shroud thermal conductance

In the fuel, clad and shroud, the time-dependent heat transfer equation is considered in integral form:

$$\frac{\partial}{\partial t}\left(\int_V h\rho\, dV\right) \;+\; \int_S \vec{\phi}\cdot d\vec{S} \;=\; \int_V p\rho\, dV\,, \tag{2.1}$$

where h and p are the enthalpy and heat source per unit mass, ρ is the density, and ϕ is the heat flux. Cylindrical symmetry is assumed and the heat flux ϕ, which is considered only in the radial direction, is expressed as

$$\left.\begin{aligned}\vec{\phi} &= \phi\vec{e}_r \\ \phi &= -\lambda\frac{\partial T}{\partial r}\end{aligned}\right\}. \tag{2.2}$$

Here, $\vec{e}_r$ is the radial unit vector, λ is the thermal conductivity of the solid, T is the temperature, and $\partial/\partial r$ denotes the partial derivative with respect to the radial coordinate.

The thermal boundary condition imposed on the fuel system is that the heat flux is zero at the center of the fuel, *i.e.* $\phi = 0$ at r=0. At the boundaries (fuel-to-gap, gap-to-clad and so on) the Newton's law of cooling is assumed, which is expressed as

$$\phi = H(T - T_0)\,. \tag{2.3}$$

That is, the heat flux out from the surface is proportional to the temperature difference between the surface and the surrounding medium. Here, T is the surface temperature, T_0 is the bulk temperature of the surrounding medium and H is a parameter called the *surface conductance* or the *surface heat transfer coefficient*.

2.1.2 Pellet-clad gap

Heat transfer across the pellet-clad gap is achieved through

1. Conduction heat transfer through the interstitial gas,
2. Convection heat transfer through the interstitial gas,
3. Solid-to-solid conduction heat transfer through pellet-clad contact points,
4. Solid-to-solid radiation heat transfer between non-contacting parts of the surface.

Hence, the radial heat flux across the gap from pellet to clad is expressed by

$$\phi \;=\; H_{gap}\left(T_{pellet} - T_{clad}\right), \tag{2.4}$$

where T_{pellet} and T_{clad} are the pellet outer surface and clad inside surface temperatures, respectively, and the gap heat transfer coefficient is given by

$$H_{gap} = H_{cd} + H_{cv} + H_s + H_r\,. \tag{2.5}$$

Here, H_{cd}, H_{cv} are the heat transfer coefficients for conduction and convection, respectively, H_s is the solid-to-solid (pellet-clad) contact heat transfer coefficient, and H_r is the radiation heat transfer coefficient.

The term H_s depends mainly on the contact pressure and the hardness of the clad tube material. In SCANAIR, the term H_{cv} is neglected, *i.e.* heat transfer due to free convection in the gas gap is not taken into account.

Comment:
The governing equation used and solved for gas conduction is a steady-state heat transfer equation. Moreover, the gas mixing is considered to be instantaneous. Accordingly, the released fission gas during the transient is assumed to mix instantaneously with the gas residing in fuel rod plena. This approximation is questionable, since there is a considerable delay time for complete mixing of released gases in the fuel rod free volume, Haste (1988). Hence, the assumption of instantaneous mixing yields a higher value of the calculated gap heat flux, than if the fission products were only partially mixed. The authors of SCANAIR have recognized this weakness, and the current model is considered for improvement, Federici *et al*. (2000b).

2.1.3 Coolant channel

The coolant channel thermal-hydraulic model is a one-dimensional enthalpy raise model. The governing equations for thermal-hydraulic calculations are thus the conservation of mass and the conservation of energy in the axial (z) flow direction. These equations are formulated in integral form. Conservation of momentum is not considered, and the coolant pressure is therefore modeled as uniform along the rod.

In the coolant channel model, the coolant is considered to be a homogenous single-phase fluid. However, boiling heat transfer in forced convection water flow (PWR conditions) and in stagnant water (NSRR[1] conditions) can be modeled. The choice between the conditions is done automatically according to the coolant flow rate.

The thermal-hydraulic models for PWR conditions comprise correlations for forced convection, nucleate boiling, critical heat flux, minimum stable film temperature, transition boiling and film boiling. The models applied for NSRR conditions include correlations for natural convection, nucleate boiling, critical flux, transition boiling and film boiling. Sodium is also modeled as a possible coolant liquid in SCANAIR, primarily for simulation of CABRI-REP-Na experiments or for fast breeder reactors.

2.1.4 Numerical method

For the fuel rod, the radial heat conduction equation in integral form is discretized in space by use of the finite volume method. The mesh consists of cylindrical rings, and thermodynamic quantities are calculated in the middle of each ring or at each node, *i.e.* at the boundaries of the rings. In the time domain, the time discretization is made by an implicit method to ensure “unconditional” stability of the solutions.

For the coolant channel, the abovementioned conservation equations, as in the solution of the radial heat conduction equation, are discretized in finite volumes. The primary unknowns are the coolant temperatures and the exit mass flow rates at each axial segment. A Newton-Raphson method is employed to solve the set of discretized algebraic equations for temperatures of the fuel rod and the coolant channel.

[1] NSRR is a TRIGA annular core pulse reactor, used in Japan for RIA simulation tests.

2.2 Structural analysis

The main objective of the structural mechanics module of SCANAIR is to calculate fuel and clad deformations. A basic assumption is that the fuel rod geometry is axi-symmetric, *i.e.*, the fuel column and the clad tube have the same symmetry axis.

The radial and axial displacements are denoted by *u* and *w*, respectively. These displacements are assumed to satisfy the following conditions:

$$\frac{\partial u}{\partial z} = 0 \tag{2.6}$$

and

$$\frac{\partial w}{\partial r} = 0\,. \tag{2.7}$$

The above conditions, which imply that shear strains can be neglected, are vindicated only if the fuel column and clad tube are sufficiently long; typically, the ratio of the cylinder length to the cylinder radius should be greater than or equal to two, *i.e.* $l/r \geq 2$. Hence, in cylindrical coordinates, based on the preceding assumptions, the strains are reduced to three components, and can be written in the form of a column matrix:

$$\boldsymbol{\varepsilon} = \begin{pmatrix} \varepsilon_r \\ \varepsilon_\theta \\ \varepsilon_z \end{pmatrix} = \begin{pmatrix} \dfrac{\partial u}{\partial r} \\ \dfrac{u}{r} \\ \dfrac{\partial w}{\partial z} \end{pmatrix}, \tag{2.8}$$

where ε_r, ε_θ and ε_z are the strain components in the radial, hoop, and axial direction, respectively.

2.2.1 Governing equations

The equilibrium relations in radial and axial directions are expressed in axisymmetric cylindrical coordinates. The radial equilibrium equation for stresses is expressed as:

$$\frac{\partial \sigma_r}{\partial r} + \frac{\sigma_r - \sigma_\theta}{r} \quad = \quad 0\,, \tag{2.9}$$

where σ_r and σ_θ are the radial and the hoop components of the normal stress, respectively. The boundary conditions imposed on this equation are that $\sigma_r = -P_f$, where P_f is the coolant fluid pressure, at the clad outer surface. At the clad inner surface and at the pellet surface, $\sigma_r = -P_i$, where P_i is the rod internal pressure. However, this boundary condition is only applied for an open pellet-clad gap, *i.e.* in absence of pellet-clad mechanical interaction (PCMI). In case of PCMI, fuel and clad is considered as a single solid cylinder, consisting of fuel and clad, and no boundary condition is applied on this interface.

Comment:
We note that equation (2.9) is a steady-state equation, meaning that inertia effects (acceleration of matter) are not taken into account. The general time-dependent equation of motion for material deformation, corresponding to equation (2.9) is:

$$\rho \frac{\partial^2 u}{\partial t^2} = \frac{\partial \sigma_r}{\partial r} + \frac{\sigma_r - \sigma_\theta}{r} \ , \tag{2.10}$$

where ρ is the material density and $\partial^2 u / \partial t^2$ is the acceleration in the radial direction. In SCANAIR, this term is ignored without any justification.

The axial equilibrium equation is obtained by writing the equilibrium condition for matter inside a global control volume, depicted in figure 3. Two situations are foreseen:

1. No PCMI:
The axial forces acting on the volume are due solely to the coolant fluid and rod internal pressures, figure 3a. In case of fuel pellets without a central hole, we have the relations:

$$\int_0^{R_{fo}} \sigma_z \, 2\pi r dr = -\pi R_{fo}^2 P_i \quad \text{for the fuel pellet,} \tag{2.11}$$

$$\int_{R_{ci}}^{R_{co}} \sigma_z \, 2\pi r dr = \pi (R_{ci}^2 P_i - R_{co}^2 P_f) \quad \text{for the clad tube.} \tag{2.12}$$

Here, σ_z is the axial stress, R_{fo} is the fuel outer radius, R_{co} is the clad outer radius, R_{ci} is the clad inner radius, and P_f is the coolant pressure.

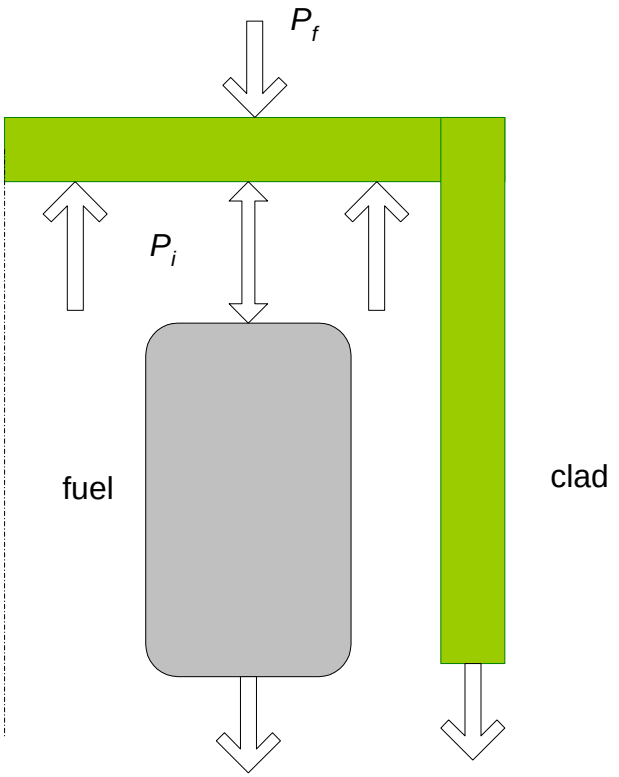

Figure 3a: Axial force balance in case of no PCMI.

2. PCMI:
In SCANAIR, axial forces due to PCMI may either be neglected (perfect pellet-clad slip), or considered by a simple model. In the latter case, fuel and clad are assumed to be perfectly stuck, *i.e*. no relative axial motion between fuel and clad is allowed in those axial segments where the fuel and clad are in contact; confer figure 3b. In this case, the equilibrium conditions in equations (2.11-2.12) are applied only on the domain above the contacting segments.

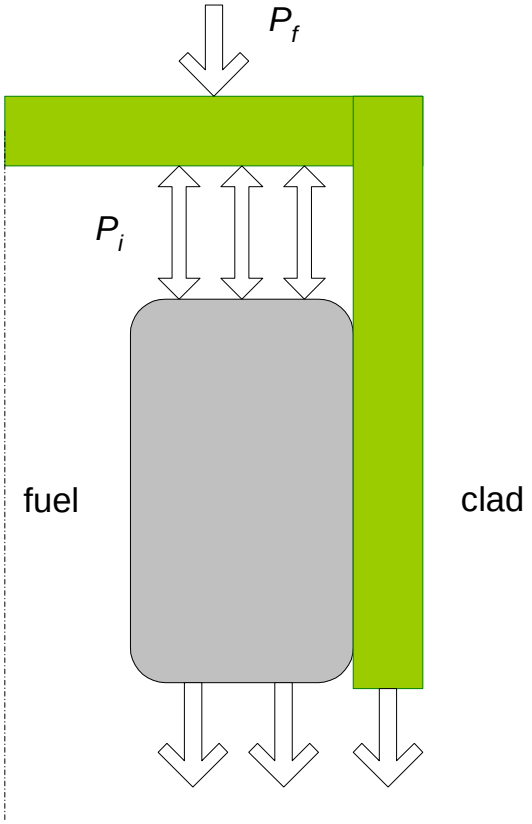

Figure 3b: Axial force balance in case of PCMI.

In addition to the axial force balance, an axial boundary condition is applied at the bottom end of the fuel rod, where there are no fuel and clad axial displacements, *i.e*. w=0 at z = 0.

2.2.2 Deformation phenomena

The SCANAIR code accounts for thermo-elastic-plastic deformation of fuel and clad. For the fuel, the code also considers contributions from fission product gaseous swelling and cracking. Below is a brief description of these models.

2.2.2.1 Fuel deformation
The total fuel strain is assumed to be the sum of thermal expansion, elastic strain, plastic strain, fission product gaseous swelling and deformation due to fuel cracking, so called pellet relocation.

Thermal expansion:
The method for calculation of thermal expansion in SCANAIR is not described. However, the material coefficient of thermal expansion is given for both solid and liquid phases of the fuel and is correlated to the fuel stoichiometry (the ratio of the concentration of oxygen atoms to that of the uranium atoms).

Comment:
For a non-uniformly heated cylinder of radius *R* with an axially symmetric temperature distribution, the radial displacement of the cylinder surface is approximately given by (Landau and Lifshitz, 1970)

$$u_{surf} = \alpha \frac{2(1+\nu)}{R} \int_0^R T(r) r dr \,, \tag{2.13}$$

where α is the coefficient of thermal expansion and ν is Poisson's ratio. If we let the cylinder be the fuel pellet column, we may estimate the surface velocity of the fuel during a step-like power pulse by taking the time derivative of u_{surf} in eq. (2.13) and relate it to the applied power and heat capacity of the fuel. If a volumetric heat source, *q(r)*, is applied at time *t*=0, the radial temperature distribution is approximately given by

$$\rho C_p \frac{\partial T(r,t)}{\partial t} = q(r) H(t) \,, \tag{2.14}$$

where C_p is the fuel heat capacity and *H(t)* is the Heaviside step function. In eq. (2.14), heat conduction in the fuel is neglected, and the approximation is therefore valid only for $t << 1$. Combining the time derivative of eq. (2.13) with eq. (2.14), we get

$$\frac{du_{surf}}{dt} = \alpha \frac{2(1+\nu)H(t)}{R} \int_0^R \frac{q(r) r}{\rho C_p} dr \,. \tag{2.15}$$

Equation (2.15) implies that the fuel surface velocity depends linearly on the magnitude of the power pulse *q(r)*. Meaning that, the greater is the RIA pulse, the larger is the pellet surface velocity.

Gaseous swelling:
Fuel expansion due to the expansion of gaseous fission products in the fuel can give considerable contributions to the fuel deformation, especially for highly irradiated fuel, during an RIA. SCANAIR accounts for the variation of fuel volume due to fission product gases residing in intergranular and intragranular gas bubbles and also in the fuel original pores. The volume occupied by bubbles depends strongly on the hydrostatic stress, $\sigma_h = (\sigma_r + \sigma_\theta + \sigma_z)/3$ in the fuel material. At equilibrium, the gas bubble pressure depends on the surface tension term and the hydrostatic stress through $P = 2\gamma/R - \sigma_h$, where γ is the surface tension of the solid and *R* is the bubble radius.

Fuel swelling (the relative increase in volume $\Delta V/V$) due to fission gases in porosity is calculated by an equation of state in the form

$$\left(\frac{\Delta V}{V}\right)_{pore} = \rho c_p \left(b + \frac{kT}{\sigma_h}\right). \tag{2.16}$$

Here, ρ is the fuel density, c_p the number of gas atom in pores per unit of fuel mass, b is the van der Waal gas coefficient for xenon, k the Boltzmann constant, and T is the absolute temperature.

Elastic deformation:
The elastic deformation of the fuel is calculated using Hooke's generalized law in an isotropic form that relates the principal stresses to principal elastic strains through Young's modulus and Poisson's ratio. These parameters are correlated to temperature and porosity of the material.

Fuel cracking:
Cracking of the fuel due to a sharp temperature gradient and non-uniform thermal expansion during power variations contributes to fuel displacements. In SCANAIR, cracks are supposed to occur in planes normal to the principal stresses σ_θ and σ_z. Only radial and axial cracks are thus modeled, and circumferential cracks are not considered.

A cracked region in the fuel is assumed not to resist tensile stresses. The strain due to cracking is thereby defined as the additional inelastic strain that must be introduced to relax a possible tensile stress to zero.

Comment:
SCANAIR does not generate cracks during the power transient. It assumes that either the fuel is already cracked, whereupon no tensile stresses can exist, or it is uncracked and assumed to have an elasto-plastic behavior. To this end, it should be noticed that the fuel gaseous swelling can be strongly affected by what assumption is made about the cracks, Latché *et al*. (1995). If the fuel is assumed cracked, σ_θ and σ_z are always zero or negative, and the hydrostatic stress σ_h in eq. (2.16) will have a different value than if the fuel were assumed as uncracked.

Fuel plasticity:
SCANAIR only considers instantaneous fuel plasticity, whereas deformation due to creep or viscoplastic deformation is neglected. Plastic strains are calculated using the Prantl-Reuss flow rule, which relates the plastic strain increment to the stress derivative of the yield function; see section 2.2.3. Plastic deformation takes place when the von Mises equivalent stress equals the flow stress, σ_0, of the material. The flow stress of UO_2 is supposed to be a function of temperature only, *i.e*., no strain hardening is considered. In SCANAIR, the flow stress of UO_2 for temperatures below T=1730°C is given by (Lamare and Latché, 1995)

$$\sigma_0 = 133.4 + T/460 \text{ [MPa]}, \qquad (2.17)$$

whereas it is assumed to be zero for temperatures above 1730°C.

Comment:
Relation (2.17) for flow stress is quite unrealistic for temperatures below 1300°C. For example, the *compressive* flow stress of UO_2 at room temperature is 960 MPa, (Glasstone and Sesonske, 1981), which is well above the predicted value of the correlation used in SCANAIR. Actually, for $T <\approx$ 1300°C, un-irradiated UO_2 is a brittle material, with no capacity for time-independent plastic deformation. Under tensile stress, it obeys Hooke's law of elasticity until a critical stress value, at which the material is torn apart by brittle fracture.

This stress is called the fracture stress, see *e.g.* chapter 11 in Olander (1976). The fuel cracking model in SCANAIR in part considers the brittle fracture, but as mentioned above, this model treats only "pre-cracked" fuel and is not able to model generation of new cracks under the transient.

At temperatures well above 1300°C, creep is a significant deformation mechanism in UO_2 fuel. Creep is not considered in SCANAIR, but the authors of the code state that the effect of fuel creep can be studied by letting the softening temperature in the flow rule (1730°C) be a tuning parameter, Lamare and Latché, (1995). Decreasing the softening temperature is thereby equivalent to increasing the effects of creep.

Moreover, the SCANAIR formulation assumes that there is no volume change during plastic deformation of the fuel. Strictly speaking, UO_2 is a porous solid and it undergoes a volume change during plastic deformation. For this reason, the plastic behavior of UO_2 is not particularly well described by the von Mises yield criterion and the Prandtl-Reuss flow rule.

2.2.2.2 Clad deformation

It is assumed that the total clad strain is the sum of strains from thermal expansion, elastic- and plastic deformation. The clad materials considered are Zircaloy, Zr-1%Nb and stainless steel.

Thermal expansion:

Thermal expansion for the clad is calculated using a correlation between the clad volumetric expansion and temperature. The correlation used for Zircaloy is the one documented in the MATPRO handbook (1979), and it caters for both $\alpha-$ and $\beta-$ phases of the Zircaloy material.

Comment:

Although the correlation for Zircaloy thermal expansion is taken from MATPRO, the correlation is not applied in its original form; SCANAIR treats the thermal expansion in α-phase Zircaloy as isotropic, which is a simplification. Moreover, SCANAIR lacks true modeling of the α-to-β phase transition kinetics; the phase transition is assumed to be instantaneous.

Elasto-plastic deformation:

For elasto-plastic deformations, the Zircaloy clad is assumed to be an isotropic material with no texture. For elastic deformation, an isotropic form of Hooke's law is used, with a simple correlation between Young's modulus and temperature. The clad plasticity model in SCANAIR is the isotropic von Mises plasticity with an isotropic strain-hardening rule, Pontoizeau (1998). The flow stress correlation for Zircaloy is only a function of temperature, and is derived from testing of irradiated stress relief anneal Zircaloy-4, commonly used as PWR fuel clad materials.

Comment:

The models used for clad plastic deformation in SCANAIR are isotropic and time-independent. While the assumption of isotropy is acceptable, the assumption of time-independence is somewhat questionable, since visco-plastic effects are pronounced in Zircaloy materials, *e.g*. Delobelle *et al*. (1996).

2.2.3 Numerical method

The fuel rod is divided into a number of axial segments. Each axial segment is treated separately, *i.e*. the mechanical equilibrium equations and material/geometrical non-linear relations are solved axial segment by axial segment. The non-linear phenomena in the system consist of evolution of plastic flow and changes in the *configuration* of the fuel, *i.e*. the closure and opening of fuel pellet cracks, the gap, and/or the pellet central hole. The core of the structural mechanics module is a solver, which computes the mechanical behavior (displacements, strains and stresses) of an axial segment for a given configuration with a set of inelastic strains. Changes in configuration and evolution of plastic strains are treated by iteration. Figure 4 is an overview of this solver.

The equilibrium equations in the radial direction of the fuel and the clad are discretized by a finite element method. The primary unknowns are the incremental displacements of each node during the considered time step. The increment of plastic strain for fuel and clad under the time step is calculated from the following two conditions:

$$\left.\begin{aligned} \sigma_{eq} &= \sigma_o \\ d\boldsymbol{\varepsilon}_p &= d\omega \frac{\partial \sigma_{eq}}{\partial \boldsymbol{\sigma}} \end{aligned}\right\}, \tag{2.18}$$

where $d\boldsymbol{\varepsilon}_p$ is the plastic strain increment, σ_{eq} is the von Mises effective stress, σ_0 is the material flow stress, and $d\omega$ is a scalar to be determined. This problem is solved by a relaxation method (also called the return method), meaning that the solutions of the equilibrium equations provide von Mises effective stress levels, which in some mesh points may be larger than the flow stress. In this situation, an increment of plastic strain is postulated, such that it shall return the value of σ_{eq} to σ_0.

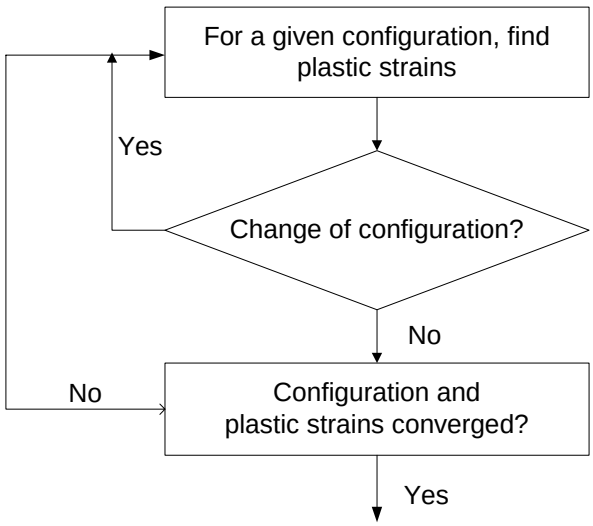

Figure 4: Flowchart for the solver for inelastic strains.

2.3 Fission gas behavior

The fission gas module in SCANAIR includes models for behavior of fission product gases in the fuel and in the free volume of the fuel rod, *i.e.* the gap, plena, and the pellet central hole, if any. The ceramic fuel UO_2, where the fission products are generated, has a granular structure. Each grain is surrounded by other grains or by (as-fabricated) cavities, called pores. Some of these pores may be open, *i.e*. they are connected to the free volume. In that case, they function as conduits, through which gas can flow to fuel surfaces.

The fission process generates fission product gases as atoms in the fuel crystal structure. The SCANAIR models do not account for gas atoms in the fuel, *i.e.* all the fission product gases are assumed to be collected into inter- and intra-granular bubbles. Hence, the diffusive migration of gas atoms in the fuel is not modeled. Nor is the migration of intra-granular bubbles to the pores. However, the transport of intra-granular bubbles into the grain boundaries and hence the formation of inter-granular bubbles, is modeled. Also the release of inter-granular bubble gas into the pores, through which it can be conveyed to the free volume, is catered for. Figure 5 is a cartoon of the fuel microstructure, as envisioned in the SCANAIR fission gas module.
In this section, we highlight some of the basic equations used in SCANAIR for modeling the aforementioned phenomena, and then close the section with some concluding remarks.

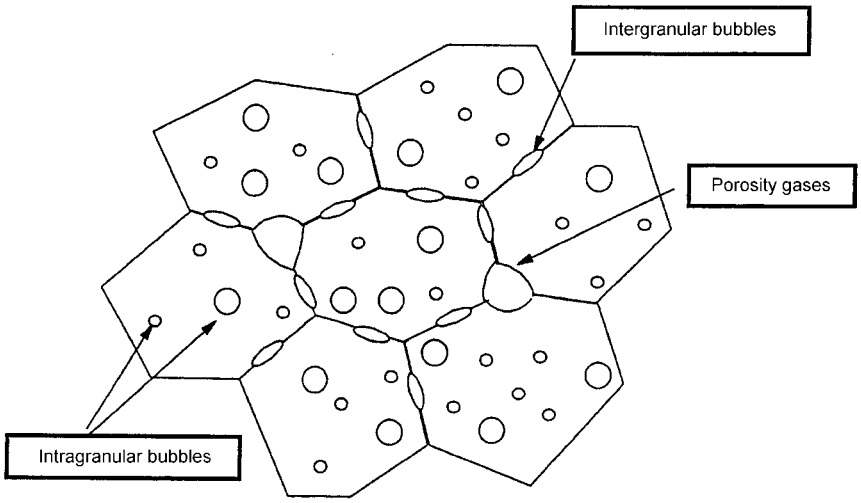

Figure 5: Fuel grains containing inter- and intra-granular gas bubbles and pores, schematically drawn. The grain size of UO_2 fuel is around 12 μm.

2.3.1 Intra-granular gas bubbles

Three phenomena are modeled for describing the intra-granular gas bubbles. These are:

- The migration of gas bubbles through the grain due to the presence of temperature gradients, and the trapping of gas bubbles in grain boundaries.
- Bubble coalescence during migration.
- Growth of gas bubbles caused by rapid diffusion of lattice vacancies into the gas bubbles, due to hydrostatic pressure exerted by the bubble to its solid surrounding.

The kinetic relation used for the migration of intra-granular gas bubbles to the grain boundaries is given by:

$$\frac{dc_{ig}}{dt} = -F_r c_{ig} \tag{2.19}$$

where c_{ig} is the gas concentration contained in intra-granular bubbles, $F_r = v_m / a$, with v_m being the gas bubble velocity, a the grain radius, and d/dt denotes time derivative. The bubble velocity is proportional to the magnitude of the temperature gradient. For bubble coalescence, SCANAIR uses Wood and Matthews's model (1979), which is based on the theory of coagulation of colloids, formulated by Smoluchowski at the beginning of the last century, see *e.g.* Chandrasekhar (1943). It considers the following relation for kinetics of intra-granular bubble concentration c_{ib}, expressed as:

$$\frac{dc_{ib}}{dt} = -F_r c_{ib} - (K_{th} + K_{br}) c_{ib}^2 \tag{2.20}$$

where $K_{th} = 4\pi r_{ib}^2 v_m \rho$, $K_{br} = 8\pi D_b r_{ib} \rho$, with r_{ib} being the gas bubble radius, D_b the bubble diffusion coefficient, and ρ the fuel density. The first term describes the rate of destruction (release) of gas bubbles, and the last term describes the coalescence by bubble migration (velocity dispersion and random diffusion).
The growth of intra-granular gas bubbles is calculated by means of the time variation of the total volume (per unit fuel mass) occupied by gas atoms in the intra-granular bubbles, N_{ib}, which may be written in the form:

$$\frac{dN_{ib}}{dt} = -(F_r - F_s) N_{ib} \tag{2.21}$$

where F_s is the swelling rate due to flux of vacancies from the fuel matrix into the intra-granular gas bubbles, which is proportional to the pressure difference between the hydrostatic stress within the fuel and the gas bubble pressure. Also, note that $N_{ib} = c_{ib} V_{ib}$, where V_{ib} is the intra-granular bubble volume. The shape of intra-granular gas bubbles is taken to be spherical.

2.3.2 Inter-granular gas bubbles

The inter-granular gas bubbles are supposed to be located on the faces of the grain boundaries, but not in the corners of the grain. They are assumed to be lenticular in shape with radius r_{eb} and dihedral angle ψ, as schematically drawn in figure 6. Furthermore, the coalescence of these bubbles is neglected. As for the intra-granular bubbles, the inter-granular bubbles are assumed to be over-pressurized with respect to the hydrostatic pressure of the fuel. Thus, growth of these bubbles is caused by flow of vacancies and the intra-granular gas bubbles into them.

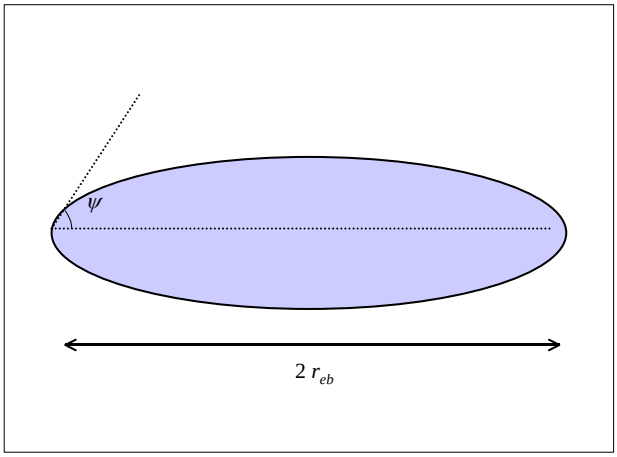

Figure 6: A lenticular shaped inter-granular gas bubble. Typically, r_{eb} = 100-200 Å.

The evolution of inter-granular gas concentration c_{eg} is described by

$$\frac{dc_{eg}}{dt} = F_r c_{ig} \,. \tag{2.22}$$

The growth of inter-granular bubble radii is expressed by

$$\frac{dr_{eb}}{dt} = (K_p + F_r K_b \frac{N_{ib}}{c_{eb}}) r_{eb}^{-2} \,, \tag{2.23}$$

where K_p is a parameter proportional to the bubble overpressure and bubble velocity, c_{eb} is the concentration (per unit mass) of inter-granular bubbles, and K_b includes geometrical factors. Equation (2.23) is attributable to Matthews and Wood (1980). The inter-granular gas can get released to the nearby pores on two conditions:

- Grain boundary gas saturation, when the grain boundary coverage reaches a certain value.
- Grain boundary rupture, when the stress due to the bubble over-pressure exceeds the material fracture strength.

When one of these criteria is met, all the inter-granular gas is immediately released into the pores and the volume of the inter-granular gas bubble is assumed to shrink to zero. From this time onward, it is assumed that there are no inter-granular gas bubbles, and that the intra-granular gas bubbles migrate directly to the grain boundary porosities.

2.3.3 Flow of gas through pores

In SCANAIR, it is assumed that the porosities and free volumes are already filled with gas at the initial state of the transient. In the porosities, the gas consists primarily of fission products. During a transient, the gas flows due to the pressure gradient in the pores. This gradient is introduced partly by the temperature gradient, but also by the burst of gas release from the gas bubbles. SCANAIR calculates only the radial flow of gas through the porosities.

The flow of gases in the porosities is given by the following integral equation for the mass balance in a volume Ω:

$$\frac{\partial}{\partial t}\left(\int_{\Omega} c_p \rho \, dV\right) + \int_{\partial\Omega} c_p \rho \vec{v} \cdot dS = \int_{\Omega} C c_{e\to p} \rho \, dV \,, \tag{2.24}$$

where c_p is the concentration of gas atoms in pores (per unit mass), ρ is the fuel density, v is the speed of the gas, $\partial\Omega$ is the area enclosing the volume Ω, and $c_{e\to p}$ is the rate of concentration of gas that is released from the grain boundaries to the pores. The velocity of fission gases in the pores is calculated from Darcy's law,

$$\vec{v} = -\mathrm{K}\nabla P_p \,, \tag{2.25}$$

where P_p is the pore gas pressure and K denotes the fuel permeability. Hence, the velocity of gas in the pores is proportional to the pressure gradient in the pores.

2.3.4 Numerical method

Three sets of kinetic equations are solved numerically for the transport of fission product gases in SCANAIR:

- Solution of intra-granular equations
- Solution of inter-granular equations
- Solution of gas flow equations in the pores

The intra-granular equations (2.19)-(2.21) are solved for each annular region of the discretized fuel separately, since these equations are space independent. The discretization in time is made by a Cranck-Nicholson scheme. The ensuing non-linear equations are solved by a Newton-Raphson method.

For the inter-granular equations, as for the intra- ones, equations (2.22)-(2.23) are solved for each annular region of the fuel separately. The time-discretized form of (2.22) is solved by a backward-Euler finite difference scheme. The ensuing non-linear equations are solved by a Newton-Raphson method.

The equations for gas flow in the pores are solved by the same token as that for the heat transfer equation in the fuel. The transport equation is solved only in radial direction. The discretization is carried out by a finite volume method on equation (2.24). The volume Ω is thereby that of a specific annular region of the fuel. The scalar variables are defined at the middle of the annular region and vectorial variables at each node, *i.e.* at the boundaries of the annulus. The resulting set of discretized algebraic equations is solved by a Newton-Raphson scheme.

Comment:
In SCANAIR, fission product gas release occurs only through migration of gas bubbles. The intra-granular gas bubbles are transported to the inter-granular bubbles due to the presence of temperature gradients, and then, upon saturation of the inter-granular bubbles, the gas is released from these bubbles to the pores. Subsequently, the gas flows through the pores to the fuel rod free volume. The gas bubbles are not transported directly to the inter-granular porosities. The reason for ignoring this process is not given in the SCANAIR documentation.

Moreover, the diffusion of gas atoms within the grain is not considered in SCANAIR. Ignoring this phenomenon limits the code to analyses of only severe transients, such as an RIA, for which the duration of the transient is usually well below 1 s. Therefore, the time processes involved consist of the time that it takes for the intra-granular gas to enter the inter-granular bubbles, the filling rate of these bubbles, and finally the flow rate of gas through channels of porosity.

Let us estimate the travel time for the intra-granular bubbles to reach the inter-granular bubbles. It can be calculated from the temperature gradient induced release rate, given by $F_r = v_m/a$, where v_m is the bubble migration velocity and a is the grain radius. Using the expression for v_m, as derived by Olander (1976) and also used in SCANAIR, we may estimate the time it takes for the bubble to travel from the grain center to the grain boundary. The expression for v_m is

$$v_m = \frac{3D_s Q\Omega^{1/3}}{kT^2 r_{ib}} \frac{\partial T}{\partial r}, \tag{2.26}$$

where D_s is the atomic surface diffusion, Q the heat of transport, Ω the volume of crystal lattice, k the Boltzmann constant, T the temperature, and r_{ib} the intra-granular bubble radius. Assuming a constant temperature gradient of $\partial T/\partial r$= 400 K/mm during the transient, a grain radius of a=5 μm, r_{ib} = 20 Å, and using numerical values for the other parameters as given in the book of Olander, (1976), we have calculated the bubble migration velocity and the travel time as a function of temperature, figures 7a-b. It can be seen that at T= 2200 K, the travel time is about 1 s.

Let us for the sake of comparison calculate the travel time for gas atom diffusion migration. Suppose we select the gas atom diffusion coefficient, which was used by Sontheimer *et al.* (1985) to evaluate transient fission gas release experiments (ramp type transients with hold time at ramp terminal levels of hours), namely the relation

$$D = 4.2\times10^{-6} \exp(-\frac{330000}{RT}) \quad [\mathrm{m^2/s}], \tag{2.27}$$

where R=8.314 J/mol·K and T is the absolute temperature. Using random walk theory, the mean square displacement can be calculated according to:

$$\bar{r}^2 = \lambda^2 \Gamma t, \tag{2.28}$$

where λ is here the distance for each jump and Γ denotes the jump frequency. Invoking Einstein's formula for Brownian motion

$$D = \frac{1}{6}\lambda^2 \Gamma \ , \tag{2.29}$$

we can express equation (2.28) as

$$\bar{r}^2 = 6Dt. \tag{2.30}$$

Putting $\sqrt{\bar{r}^2} = a$, the travel time for gas atom can be estimated via

$$t = \frac{a^2}{6D}. \tag{2.31}$$

We have plotted the gas atom diffusion travel time versus temperature by substituting relation (2.27) for D in equation (2.31), figure 8. The results can be compared with figure 7b. As can be seen, at T=2200 K, t= 68 s compared to 1 s for the intra-granular bubble travel time. Thus, neglecting the gas atom diffusion during severe transients such as RIA is permissible. However, SCANAIR cannot be used to evaluate fission gas release during mild transients, such as ramp experiments that have been performed in the STUDSVIK and the RISØ reactors.

(a)

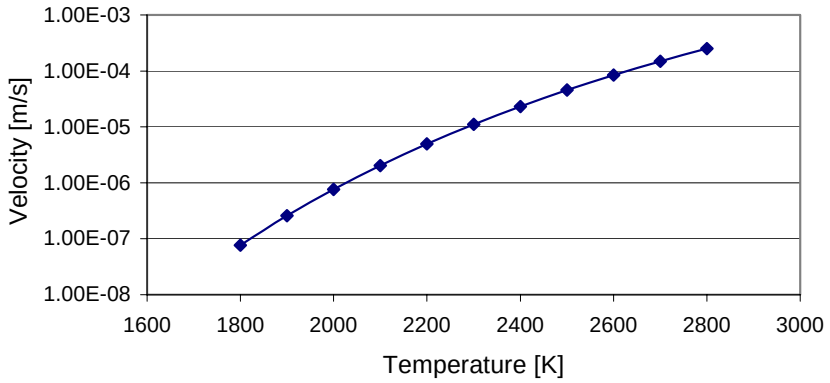

(b)

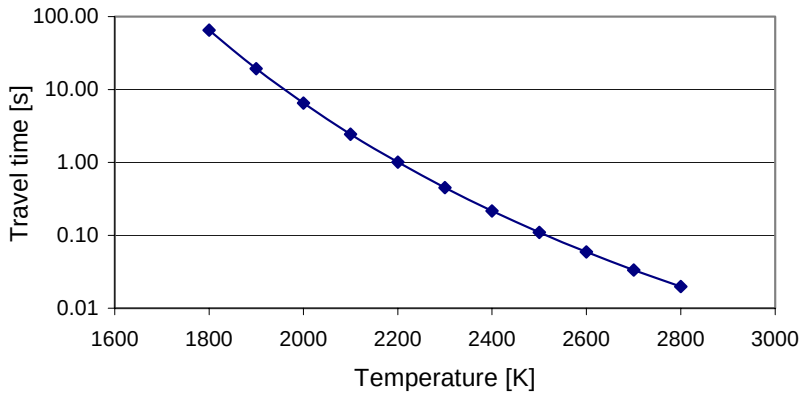

Figure 7: Migration velocity and travel time of an intra-granular bubble in UO_2 grain as a function of temperature at a constant temperature gradient of $\partial T/\partial r$= 400 K/mm during the transient. Grain radius of a=5 μm and bubble radius r_{ib} = 20 Å are assumed.

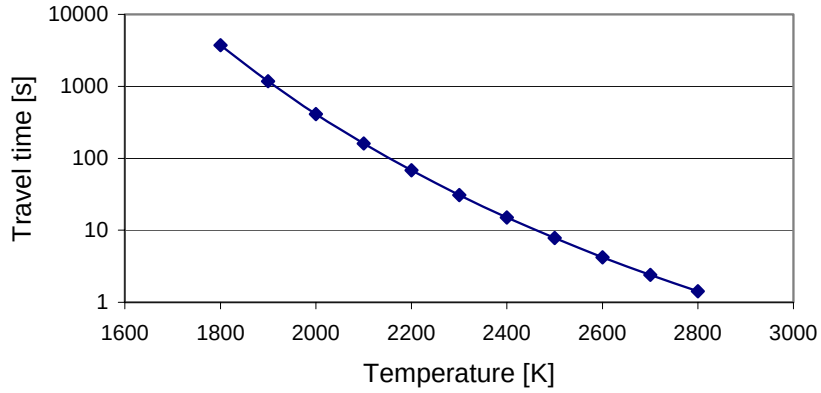

Figure 8: Travel time of a gas atom in a UO_2 grain with a radius of a=5 μm.

3 SCANAIR interface: input and output data

SCANAIR is intended for modeling the thermal-mechanical fuel behavior under RIA, and does not comprise steady-state models for calculation of the fuel behavior prior to the transient. The base irradiation must therefore first be modeled by use of a steady-state fuel performance code, and the predicted fuel rod conditions transferred to the SCANAIR input deck, where they constitute initial conditions to the RIA. At present, the SCANAIR code has two pre-processor tools (TOSCAN and METEOSCAN) for convenient creation of SCANAIR input from output of the fuel rod analyses codes TOSURA and METEOR, respectively. The output from SCANAIR consists of

- A summary output file with primary fuel parameters in text format
- Binary warning messages on numerical problems and events encountered under calculation
- Several binary data files used for creation of graphs or alphanumeric tables

Post-processing tools are available for handling the binary output files, *e.g.* for plotting selected fuel rod parameters with respect to time or spatial position. In this section, we briefly review the input/output capabilities of the code. The full description of these capabilities and the input details are provided in the SCANAIR reference manual, Lamare (2001).

3.1 Input data to SCANAIR

The initial conditions for RIA analysis, *i.e.* the state of the fuel rod prior to an RIA, must be supplied from output of a general fuel rod thermal-mechanical code. At present, the SCANAIR code is designed to read such data from the codes TOSURA or METEOR via the interface programs TOSCAN and METEOSCAN. Through these interfaces, some data are read for the hot state of the fuel and others for the cold state. For the hot state, SCANAIR reads:

- End-of-life radial and axial fuel temperature profile
- Radial and axial power profile

For the cold state, the following parameters are read

- Fuel and clad radii and axial positions
- Radial distribution of plutonium concentration, burnup, stoichiometry, gas concentration, porosity and density of the fuel
- Gap gas components and concentrations

A calculation with SCANAIR is preferably initiated from cold state, since starting from a non-zero power may lead to differences between the hot state initial conditions calculated by SCANAIR and those from the pre-irradiation code (Lamare, 2001).

The input deck to SCANAIR is organized in blocks or structures, in which keywords are used for entering input parameters. The input syntax is clear and logical, and the syntactical correctness of all input data is checked by the SIGAL tool (Jacq, 1998). The default unit system for physical parameters is SI, but the pre-processor tool SIGAL handles most units. When departing from SI-units, the unit must be specified after the value entered in the input file. For example, `4.mm`, will translate to 0.004 m. The list of main input structures in SCANAIR is shown in Table 3.1 below.

Table 3.1: Important input data structures to SCANAIR

Structure	**Task**
TIME MANAGEMENT	Time stepping and output instructions
POWER	Power history during transient
FUEL	Irradiated fuel material characterization
CLAD	Irradiated clad material characterization
GAP	Fuel-clad gap characterization
MESHING AND GEOMETRY	Meshing instructions for fuel and clad
PHYSICAL PROPERTIES	Material physical property data for fuel/clad
FLUID	Coolant properties
WALL	Thermal calculation of the shroud wall of the core
BY-PASS	Thermal outer boundary condition

An important block in Table 3.1 is the `STRUCTURE POWER`, in which the power history during the transient and the power distribution profiles are defined. The axial and radial power profiles are assumed to be constant during the transient, and the relative power distribution is defined within the `STRUCTURE POWER` input block. The local power in a certain position is obtained by multiplying the relative power distribution with the total rod power at a given point in time. The total rod power as a function of time can be defined either as a simple time history table with power listed versus time, or in terms of the injected energy at a specific point in time. In the latter case, the radial average injected energy E_{inj} [J/g] in the peak power axial segment at time t_s [s] is specified, together with a dimension-free time history *f(t).* The fuel rod total power at time *t* is then defined through

$$p(t) = P_T \, f(t) \ , \tag{3.1}$$

where P_T is calculated internally by SCANAIR through

$$P_T \ = \ \frac{E_{inj} \, m_{fuel}}{Z \int_0^{t_s} f(t) dt} \ . \tag{3.2}$$

Here, m_{fuel} is the fuel total mass, calculated from the input fuel density and volume, and Z is the axial peaking factor. It should be noticed, that the power pulse shape $f(t)$ is expected as input to SCANAIR, and must be based either on experimental data or calculations with an neutronics code.

3.2 Output data from SCANAIR

The output files created by SCANAIR are divided into 3 types

- A summary listing file with primary fuel parameters in text format
- Binary warning messages on numerical problems and events encountered under calculation
- Several binary data files used for creation of graphs or alphanumeric tables

An event is defined as a transition from one state to another, *e.g.* closure of the pellet-clad gap in an axial segment. In the summary output, many detailed fuel and clad physical data are listed as a function of time and spatial position. Some data of particular interest for fuel and clad are stated in Table 3.2.

Table 3.2: Some quantities listed in SCANAIR summary output file `listing.txt`

Fuel	Clad
Radial temperature distribution	Radial temperature distribution
Radial distribution of principal stresses	Radial distribution of principal stresses
Radial distribution of effective stress	Radial distribution of effective stress
Radial distribution of principal plastic strains	Radial distribution of principal plastic strains
Radial distribution of principal elastic strains	Radial distribution of principal elastic strains
Radial distribution of thermal strains	Radial distribution of thermal strains
Plastic strain energy density [1]	Plastic strain energy density [1]
Enthalpy	
Swelling strain	
Cracking strain	
Fission gas concentration in fuel	
Gas bubble concentration	
Gas bubble radii	
Swelling of gas bubbles and pores	
Gas saturation of inter-granular bubbles	

The summary output also includes the following quantities of interest, listed as functions of time. These quantities are either given for each axial segment of the rod or as rod averaged values:

- Average injected energy [J/g]
- Average deposited energy [J/g]
- Average enthalpy [J/g]
- Pellet clad contact pressure [Pa]
- Free volume pressure [Pa]
- Free volume gas composition
- Rod average fission gas release

[1] Plastic strain energy density is defined as: $w_{pl} = \int \sigma \, d\varepsilon_{pl}$ where σ is the effective von Mises stress and $d\varepsilon_{pl}$ is the increment of effective plastic strain.

Various post-processing tools are available for handling the binary output files. As an example, for plotting selected fuel rod parameters with respect to time or spatial position, the SIGAL tool TIC is used. Although TIC seems to be an efficient graphic tool of general character, at Quantum Technologies, we have appended the general graphic tool X-manager to SCANAIR, since we have found it to be friendlier and more flexible to use.

4 Code implementation and documentation

4.1 Code implementation

The SCANAIR code is written in Fortran-77. The code makes extensive use of the utility program SIGAL, which is also written in Fortran-77, Jacq (1998). SIGAL is used for allocation, storage and handling of data structures, and also for pre- and post processing of data. The computational flow in SCANAIR is presented in figure 9.

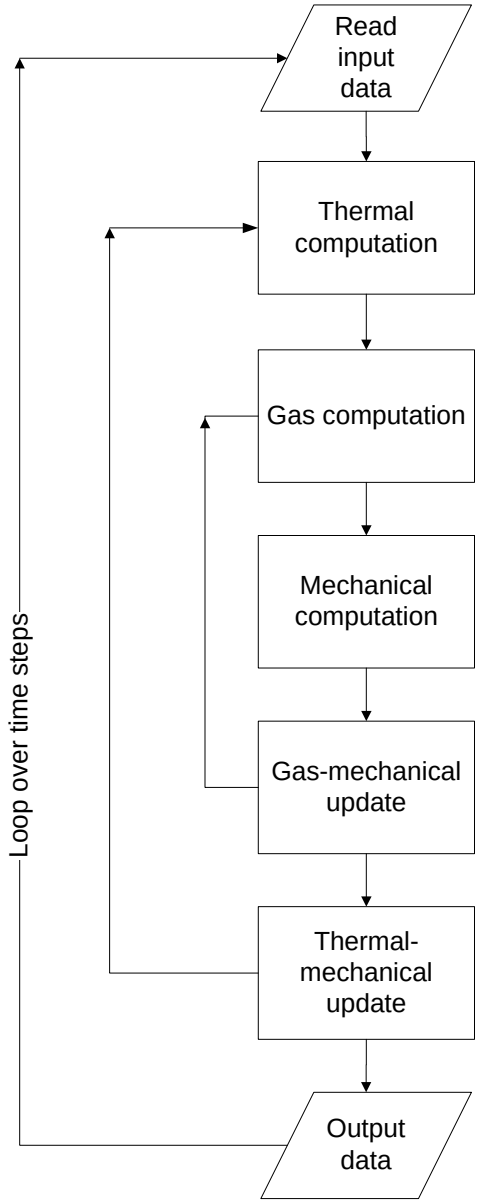

Figure 9: Flowchart of the SCANAIR main program.

The SCANAIR programming style in Fortran-77 is consistent and has good quality. It follows a set of programming rules regarding legibility, maintenance and portability. The code subroutines contain adequate amount of comments, which facilitate both maintenance and extension, Lamare and Latché (1995).

A drawback with SCANAIR in its present form, is that the code is tied to computers running POSIX-like operating systems, such as UNIX or Linux. The reason for this confinement is that the code and its pre- and post-processors are executed and controlled by use of shell scripts, written in the UNIX C-shell scripting language. At present, SCANAIR can thus not be run under the Microsoft Windows operating system.

4.2 Code documentation

The documentation related to SCANAIR is in general of good quality. At present, there are basically 3 documents describing the code and its use:

1. An original theory manual and model description, which was released together with version 2.2 of SCANAIR (Lamare and Latché, 1995).
2. A reference manual, accompanying version 2.3 of the code (Lamare, 1998). This document shortly describes modifications to the code introduced in version 2.3, and also provides a user's manual with a description of input and output.
3. A reference manual, accompanying version 3.2 of the code (Lamare, 2001). This document shortly describes bug fixes and modifications to the code introduced in version 3.2, and also provides a completely revised user's manual.

The theory manual and model description to the present version of SCANAIR (3.2) is thus scattered over three different reports, which is inconvenient. A comprehensive document, describing the current state of the code, is therefore desirable.

The current user's manual (Lamare, 2001) is well written, and together with examples of SCANAIR input files provided by IPSN, the code is comparatively easy to use. Documentation on verification and validation of the code is unfortunately weak; to our knowledge, there are no reports describing testing, verification and validation of the SCANAIR code, although some results of such work have been presented at international meetings and conferences, *e.g*. by Papin *et al*. (1997).

In addition to the documentation related directly to SCANAIR, there are also several documents describing the pre- and post-processors TOSCAN, METEOSCAN, and TIC. This is also true for the utility program SIGAL (Jacq, 1998).

5 Computations

Version 3.2 of the SCANAIR code was successfully installed in a Personal Computer (PC) environment, utilizing versions 7.0 and 7.1 of the Red Hat Linux operating system. A number of computations with SCANAIR were performed for the purpose of evaluation, verification and validation, and the results are presented in this chapter and relating appendices.

The verification computation is an RIA simulation test case, named REP4, which was provided to us by the developers of SCANAIR at IPSN/SEMAR in the *Centre d'Etudes de Cadarache*, France. The case was studied in detail and the results are documented in section 5.1 and appendix A. The rather extensive documentation of this case serves primarily for recognizing the capability of the code and its response, but it also serves as a well-documented reference case, which can be used to verify future code versions.

Some of the SCANAIR results on the REP4 test case have also been compared with those obtained from calculations with the STRUCTUS code. The comparison, the results of which are presented in section 5.2, was made in order to independently verify the thermal-mechanical solution methods applied in SCANAIR.

Next, SCANAIR was used to simulate a ramp test performed at Studsvik, namely, a test rod from the TRANS-RAMP IV project. Although SCANAIR is not designed to simulate such ramp experiments, we have applied it anyway, in order to get a realization of the limitation of the SCANAIR applicability. Results from this analysis are compared with experimental test data in section 5.3 and appendix B. Finally, a few SCANAIR results obtained from simulation of the test rod REP-Na2 are presented in section 5.4. The rod belongs to one of the RIA tests series, REP-Na, made in the French CABRI test reactor.

5.1 REP4 test case

The test case REP4 is a hypothetical transient case, used primarily for verification of SCANAIR installation and compilation. For us, it also functions as a reference test case, to which future versions of the code can be compared. Documentation of this test case is therefore important for the quality assurance of the code. Rod REP4 originates from a 17×17-array PWR rod, which has been pre-irradiated for 4 years. The segment of the rod that is subjected to a transient simulation had an average burnup of 7.44 atom%, corresponding to an exposure of about 69.5 MWd/kgU. The main data characterizing fuel rod dimensions and conditions prior to ramp are presented in Appendix A.

The pre-irradiation calculation was performed by IPSN, using the code TOSURA. In the pre-irradiation calculation, the rod was discretized by dividing it into three axial segments for both fuel and clad, 20 radial rings for the fuel, and six radial rings for the clad tube. The outermost ring of the tube represented the oxide layer. In the subsequent analysis with SCANAIR, each axial segment of the rod used in the pre-irradiation calculation was split into 4 segments. That is, the SCANAIR computation was performed for 12 axial segments. In addition, the fuel radial mesh in SCANAIR was extended to 28 rings, with a refinement in the fuel rim region.

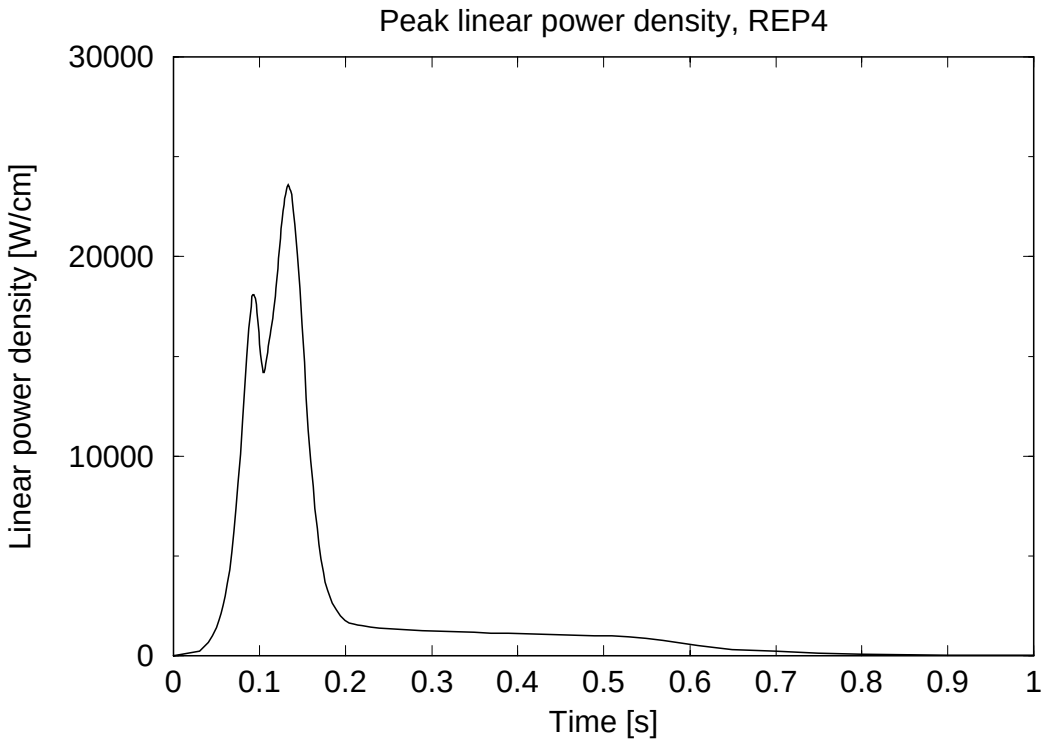

(a)

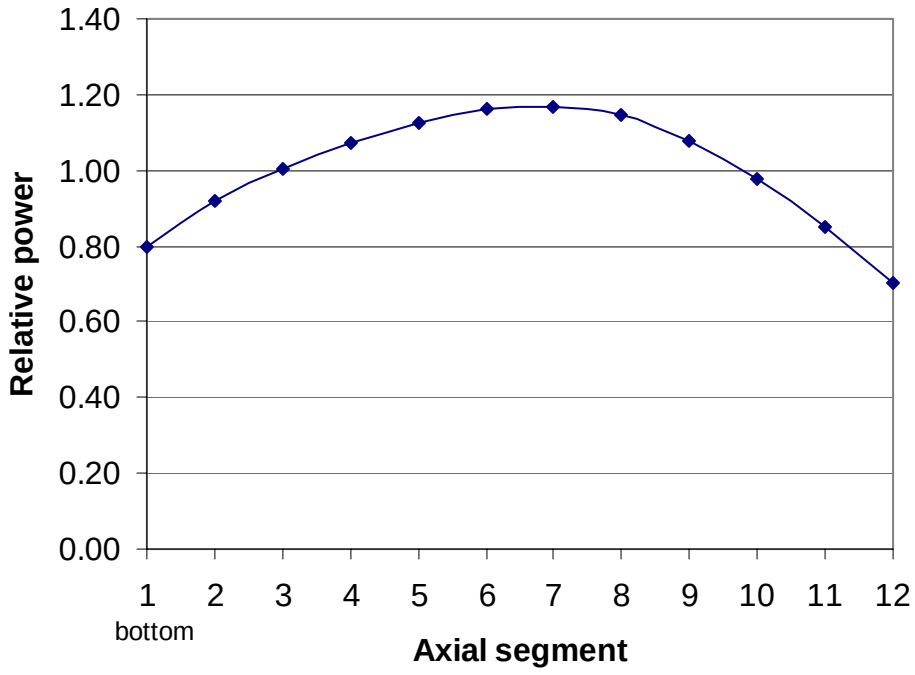

(b)

Figure 10: Transient power history for the test case REP4, (a) axial peak linear power density versus time, (b) axial power distribution, kept constant during the transient.

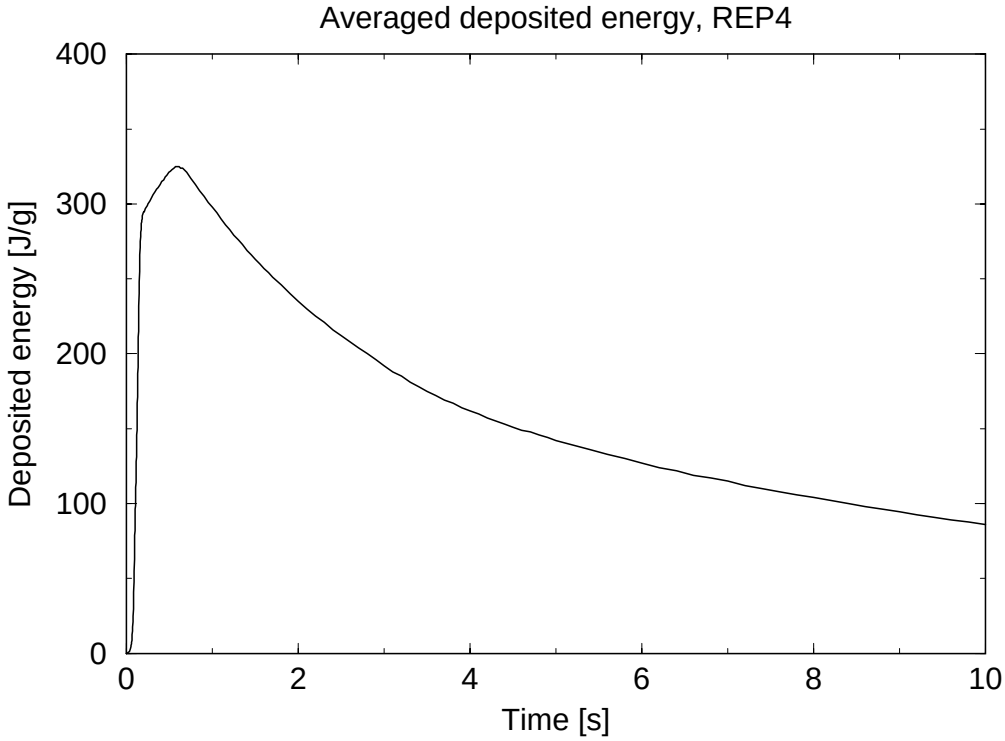

(a)

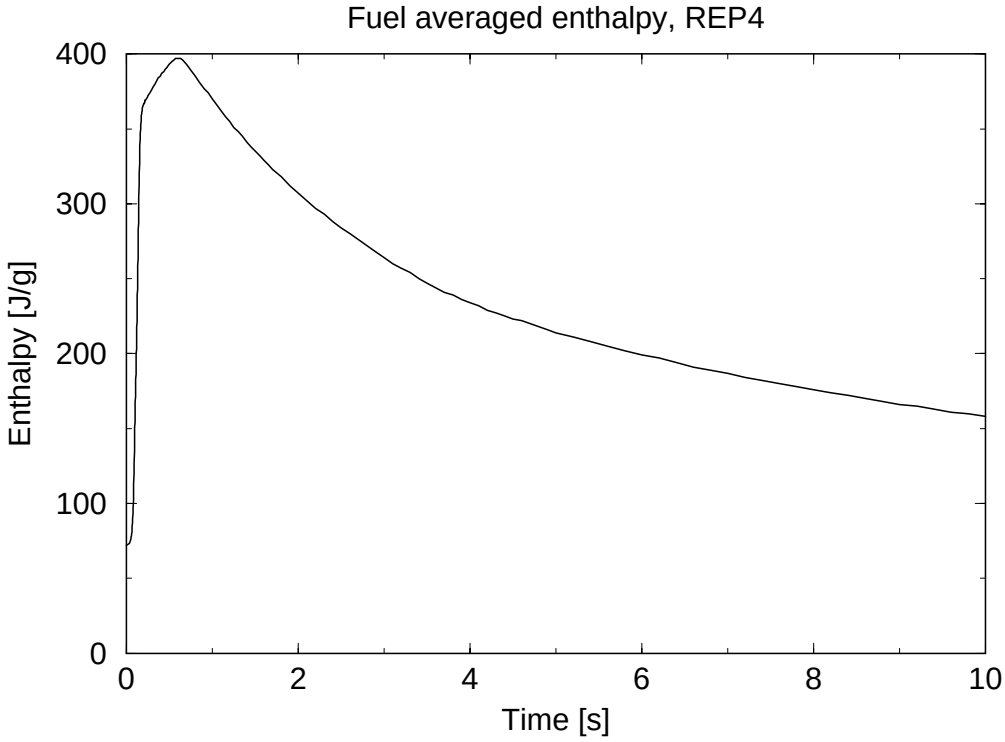

(b)

Figure 11: Fuel rod axial peak radial average input energy quantities versus time during the transient, (a) deposited energy (absorbed heat), (b) enthalpy.

The transient power history that the fuel rod is subjected to is presented in figure 10a. The figure shows the peak linear power density, which corresponds to axial segment 7 from rod bottom; the constant axial power profile used throughout the transient is shown in figure 10b. The corresponding plots for the *axial peak (i.e. segment 7) radial average* deposited energy and enthalpy versus time are shown in figures 11a and 11b, respectively. In this transient simulation, the coolant is liquid sodium with inlet temperature 281°C, inlet mass flow rate 0.308 kg/s, and a uniform pressure of 0.46 MPa.

***Results**:*
The clad outer surface temperature and rod free volume pressure, calculated versus time by SCANAIR, are plotted in figures 12 and 13, respectively. Other output data of interest; relative power, plutonium concentration, burnup, fuel temperature, fuel swelling, as a function of fuel radius, are presented in appendix A. Also the calculated hoop plastic strain, hoop stress, and plastic strain energy density across clad are shown in appendix A.

***Discussion**:*
The clad surface temperature, figure 12, reaches its peak value (352°C) at about 0.5 s from the start of the transient. Note that the linear power density reaches its peak at around 0.15 s, figure 10a. From figures 13a and 13b, we notice a substantial raise in rod internal pressure from 5.7 bar to 110 bar in a period of about 0.2 s, due to a rapid release of fission product gases. The fission gas content in the fuel porosity prior to the transient controls the gas release during the transient in SCANAIR. In input, the pore pressure (calculated by a steady-state fuel modeling code) is specified, and the van der Waals gas equation of state is then used in SCANAIR to calculate the associated fission gas content. The input pore pressure for the test case was 11.71 MPa.

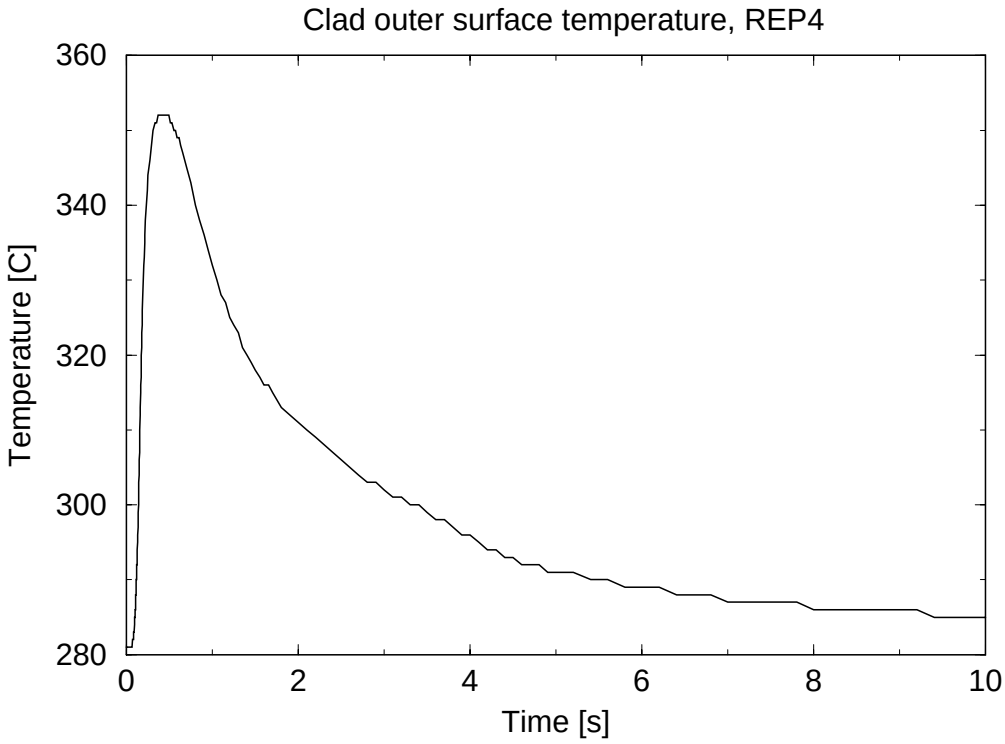

Figure12: Axial peak clad surface temperature versus time during the transient as calculated by SCANAIR.

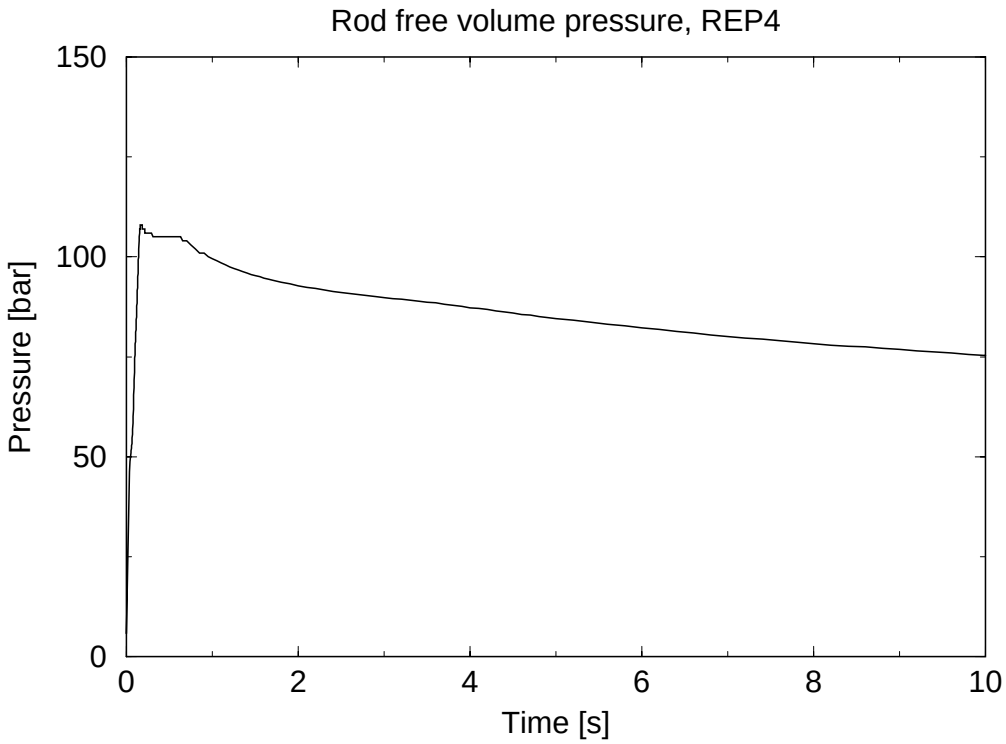

(a)

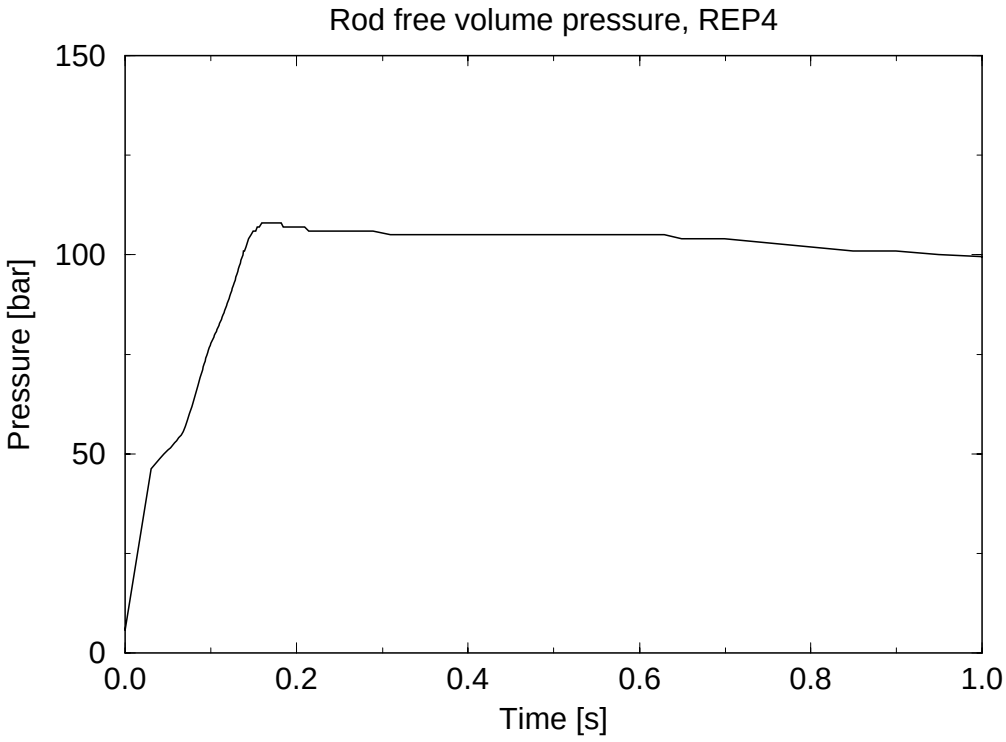

(b)

Figure13: Rod internal pressure versus time during the transient, as calculated by SCANAIR at different time scales, 1 s and 10 s.

5.2 Comparison of SCANAIR with STRUCTUS

The reference test case REP4, described in the previous section, has been used for a brief independent verification of SCANAIR. The verification was made by comparing key fuel rod parameters predicted by SCANAIR with those computed by STRUCTUS; a code for analyses of fuel rod thermo-mechanical behavior under RIA, currently under development at Quantum Technologies, (Massih and Jernkvist, 2001).

Like SCANAIR, STRUCTUS must be supplied with burnup-dependent initial conditions generated by a fuel performance code with steady state modeling capability. For the considered test case, the initial conditions generated by TOSURA were used in both SCANAIR and STRUCTUS; see appendix A. More specifically, the initial conditions supplied to STRUCTUS were the rod geometrical data for axial elevation 378.4 mm in table A1, and the radial power distribution in figure A1. The applied power history is defined in figure 10a.

In STRUCTUS, the fuel rod behavior at one single axial position is modeled. As a consequence, the code lacks the possibilities to model the variation in coolant conditions along the fuel rod and the mixing of released fission gases within the rod. For this reason, the following methodology was applied when comparing the results of SCANAIR with those of STRUCTUS:

1. Only the peak power axial segment was considered in the comparison. This corresponds to segment 7 in the SCANAIR analysis presented in section 5.1.
2. The time-dependent coolant conditions applied in STRUCTUS were those calculated in the peak power axial segment by SCANAIR. These coolant conditions are defined by the coolant temperature and clad-to-coolant heat transfer coefficient, presented in figures A6 and A7.
3. The pellet-to-clad gap heat transfer coefficient applied in STRUCTUS was the one calculated in the peak power axial segment by SCANAIR. The heat transfer coefficient (H_{gap} in equation 2.5) is given as a function of time in figure A8. The sudden decrease in H_{gap} is due to rapid release of accumulated fission gas during the early part of the RIA.

Results:

The fuel centerline temperatures predicted with SCANAIR and STRUCTUS are compared in figure 14, whereas figure 15 shows the predicted temperatures at the fuel pellet surface as function of time. Figure 16 shows the radial temperature gradient in the fuel at time t=0.133 s; this point in time corresponds to the maximum heat generation rate under the RIA (23600 W/cm in the peak power axial segment; confer figure 10a). The calculated pellet-clad contact pressure was also compared between the two codes. This parameter is of interest, since it is strongly affected by models for the deformation behavior of both fuel and clad. The result is shown in figure 17.

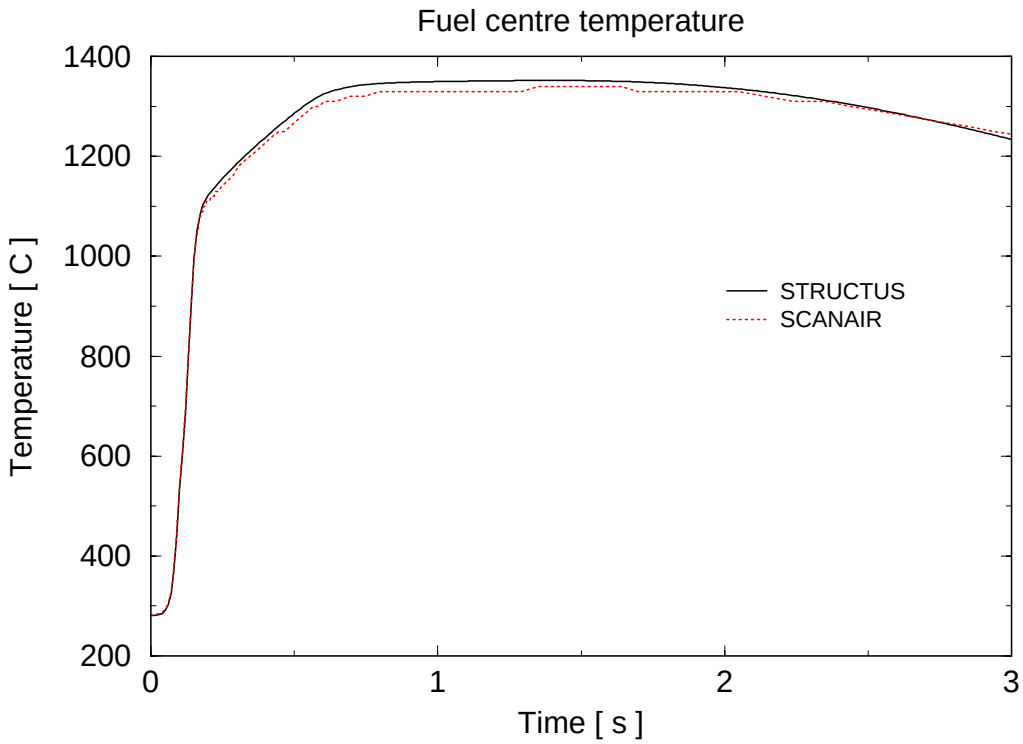

Figure 14: Comparison of predicted fuel centerline temperature in the peak power axial segment under the REP4 transient.

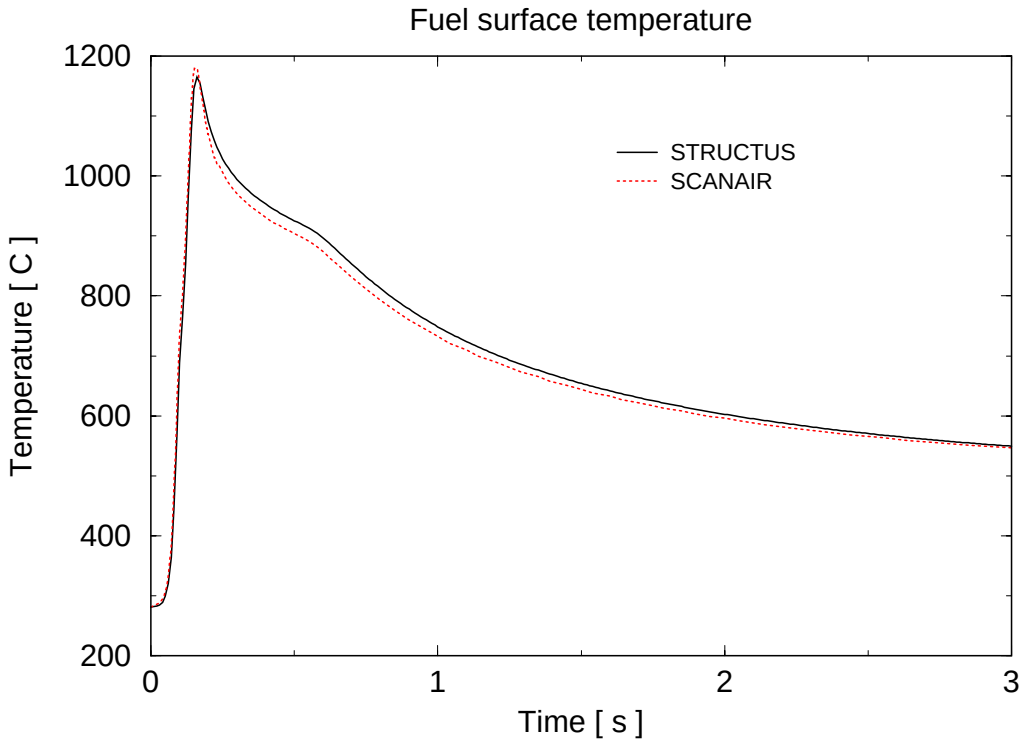

Figure 15: Comparison of predicted fuel pellet surface temperature in the peak power axial segment under the REP4 transient.

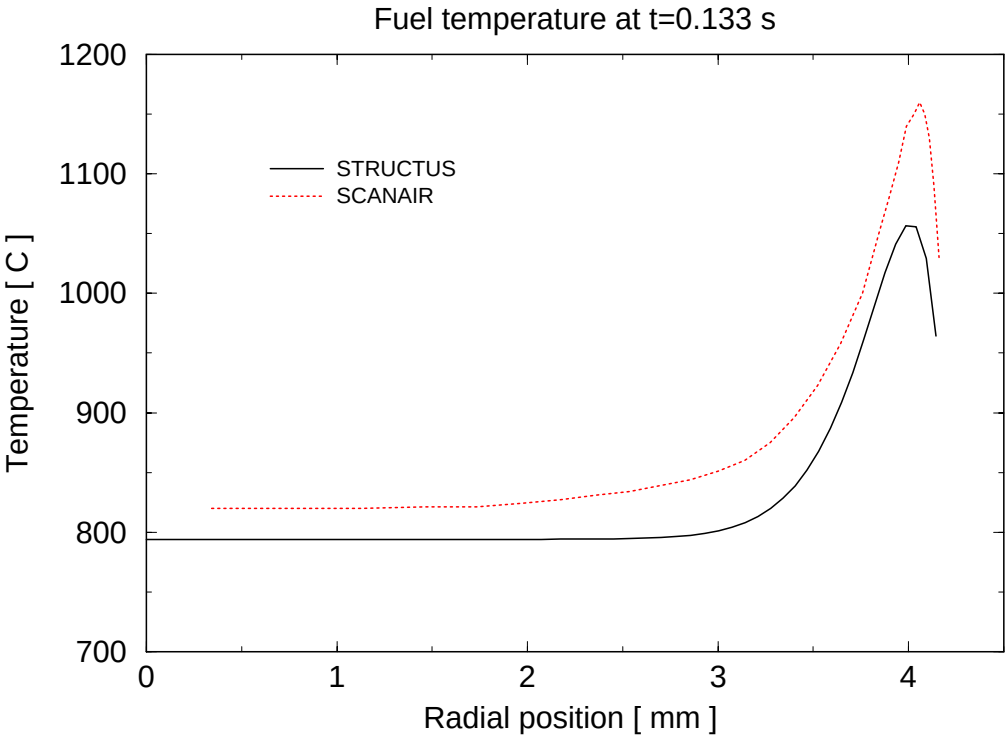

Figure 16: Comparison of predicted fuel radial temperature gradient in the peak power axial segment under the REP4 transient.

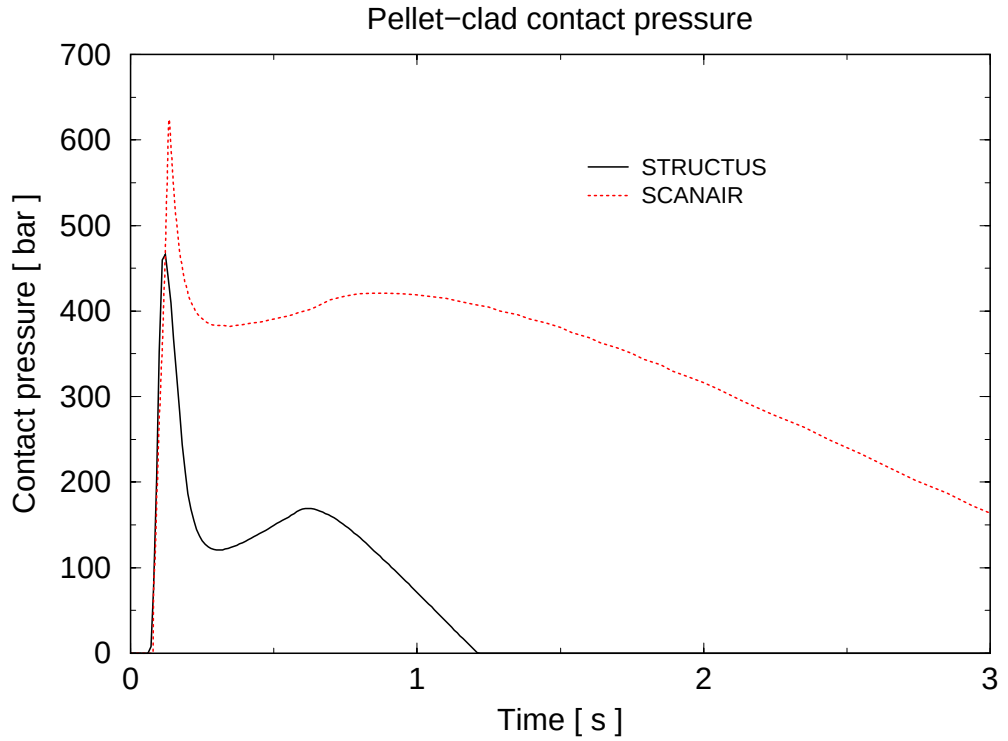

Figure 17: Comparison of predicted pellet-clad contact pressure in the peak power axial segment under the REP4 transient.

Discussion:

As evidenced by the figures, the agreement in calculated fuel rod thermal behavior between SCANAIR and STRUCTUS is good, whereas the predicted mechanical behavior (here represented by the pellet-clad contact pressure) exhibits large differences. Calculated fuel temperatures differ by at most 5%, which is surprisingly good, considering that models for material thermal conductivity and heat capacity differ between the codes.

In mechanical analyses, correlations for thermal expansion and elasto-plastic properties of fuel and clad differ between SCANAIR and STRUCTUS. However, the most important differences between the codes with respect to mechanical analyses are found in the modeling of gaseous fission product swelling and cracking of the fuel. These deformation mechanisms are considered in SCANAIR but not in the present version of STRUCTUS. Consequently, the radial expansion of the fuel and also the pellet-clad contact pressure predicted with SCANAIR will be larger than those calculated with STRUCTUS.

The two codes also differ with respect to numerical methods applied in the solution of the coupled thermo-mechanical problem. However, these differences should not significantly affect the predictions, provided that the numerical methods are correctly implemented.

5.3 TRANS-RAMP IV test case

In this section, we employ the SCANAIR code to simulate a fuel rod, which was tested in the TRANS-RAMP IV (TR-IV) project at Studsvik. The rod under consideration is rod Q11/3, (Djurle, 1993). Actually, there are two reasons that make this exercise somewhat inept. Firstly, as discussed in section 2.3, SCANAIR is not designed to simulate transients such as the TR-IV tests, which are slow and low-power events relative to postulated RIA transients. Secondly, the base-irradiation data needed for SCANAIR input could not be closely generated, simply because we do not at present have access to a steady-state code, by which such input data for SCANAIR could be produced. Nevertheless, we carry out this exercise in order to get a realization of the limitation of the SCANAIR applicability.

Using hand-calculations based on data from Djurle's report and technical judgment, we have produced simplified input data for the TR-IV rod Q11/3, which we believe are fairly representative for the conditions of the rod before the power ramp. The rodlet under consideration belonged to a full-size fuel rod that was irradiated in the GRAVELINES 3 PWR in France. The test rods in TR-IV had operated in GRAVELINES 3 for 305 effective full power days and were standard 17×17-array type rods, designed for use in 900 MWe PWRs.

Rod Q11/3 was re-fabricated for testing, and it was thereby refilled with helium gas to a pressure of 2.5 MPa. The fuel material was UO_2 and the clad was made of stress relief anneal Zircaloy-4. The ramp test was carried out by bringing the rod to a linear power density of 46.5 kW/m and interrupting the test 40 s after the start of the transient. There was no indication of clad failure. The ramp test was performed at the Studsvik R2 reactor at a loop pressure of 14.6 MPa and a coolant inlet temperature of 311 to 314°C. The ramp rig used for the test was a helium-3 rig equipped with an elongation detector, Djurle (1993).

A number of post-ramp examinations were made on rod Q11/3, (Djurle, 1993), but here we only call attention to the rod profilometry measurement and fission gas release measurement. The results of clad profile traces for the rod is given in figure 10.4 of Djurle (1993) and reproduced here for the reader's convenience in figure 18. It can be seen that a maximum diameter increase of around 20 μm, corresponding to a plastic strain of 0.21 %, occurred in this cladding during the ramp.

Rod Q11/3 was the only intact rod in the TR-IV program, and hence, the fission gas release was determined for this rod. Destructive examination of the rod after the ramp showed a release fraction of 0.005. We note, that since the rod was re-fabricated and filled with helium, all the gas release emanated from the ramp and nothing from the base irradiation, Djurle (1993).

In SCANAIR, rod Q11/3 was modeled by dividing it into 12 axial segments for fuel and clad, 18 radial rings for the fuel and six radial rings for the clad tube. The outermost ring of the tube represented the clad oxide. In this ramp simulation, the coolant is water with inlet temperature 281°C, inlet mass flow rate 3.5 kg/s and a pressure of 14.6 MPa. The ramp power history utilized for the SCANAIR input is reconstructed from figure 9.9 of Djurle (1993), and plotted in figure 19. Other pre-ramp data on the rod, used as input to SCANAIR, are given in appendix B.

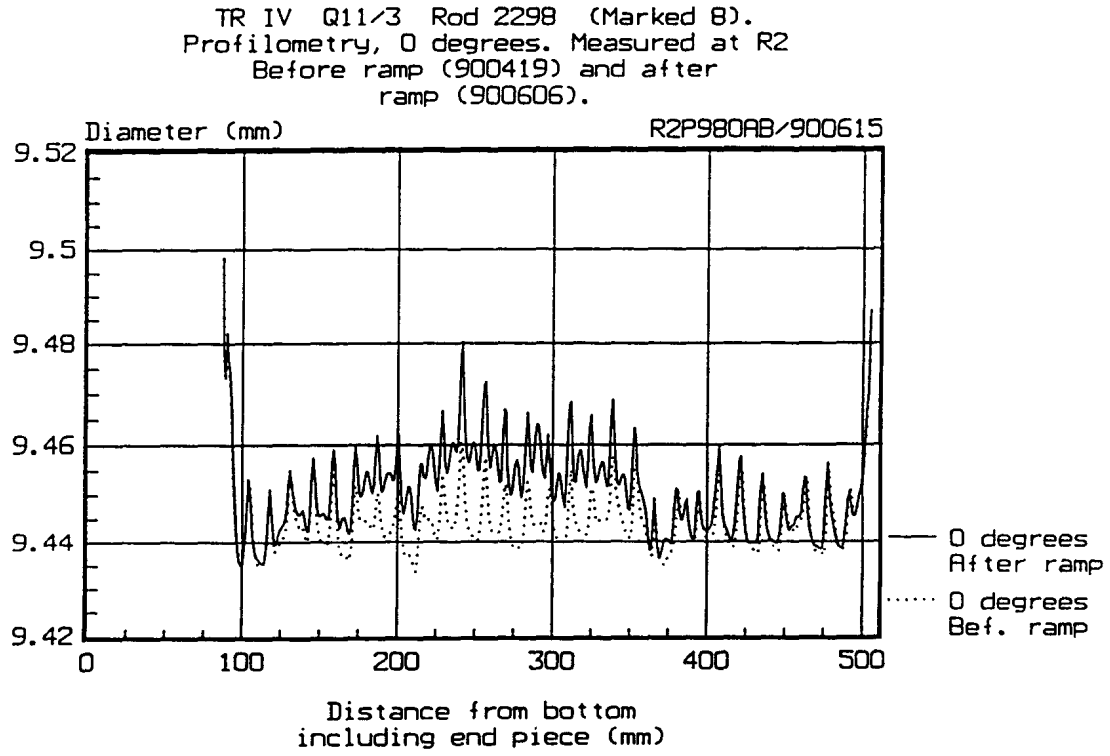

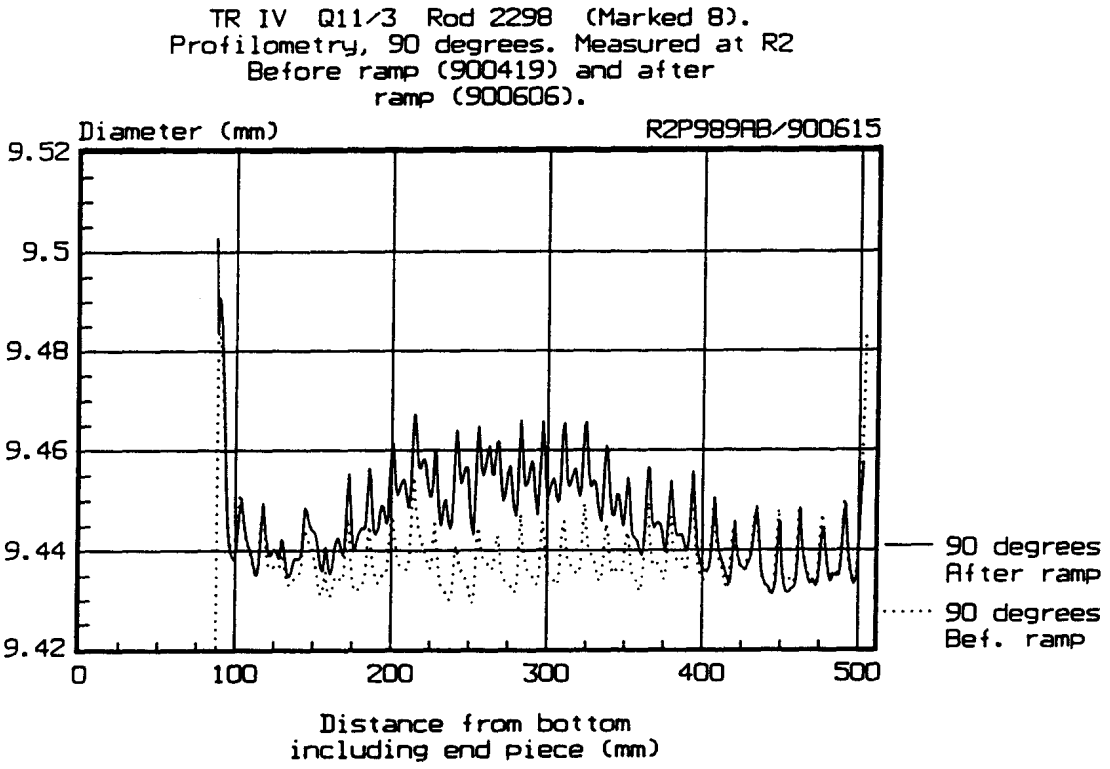

Figure 18: Profilometry of rod Q11/3 at two circumferential positions, 0 and 90°, before and after the ramp test made at Studsvik. After Djurle (1993).

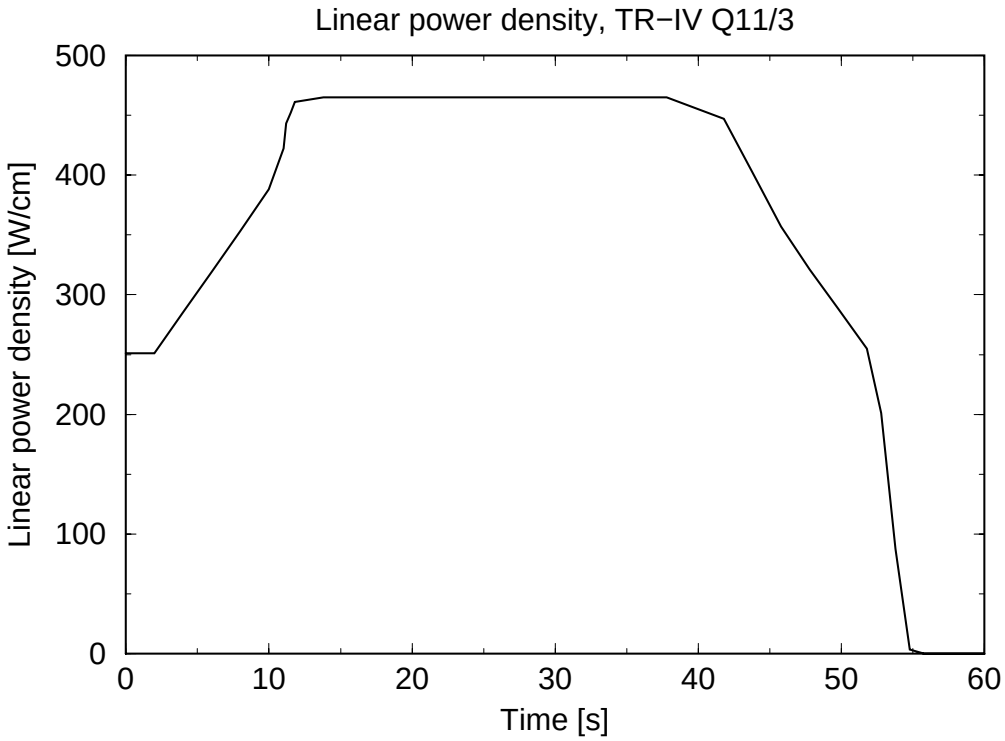

(a)

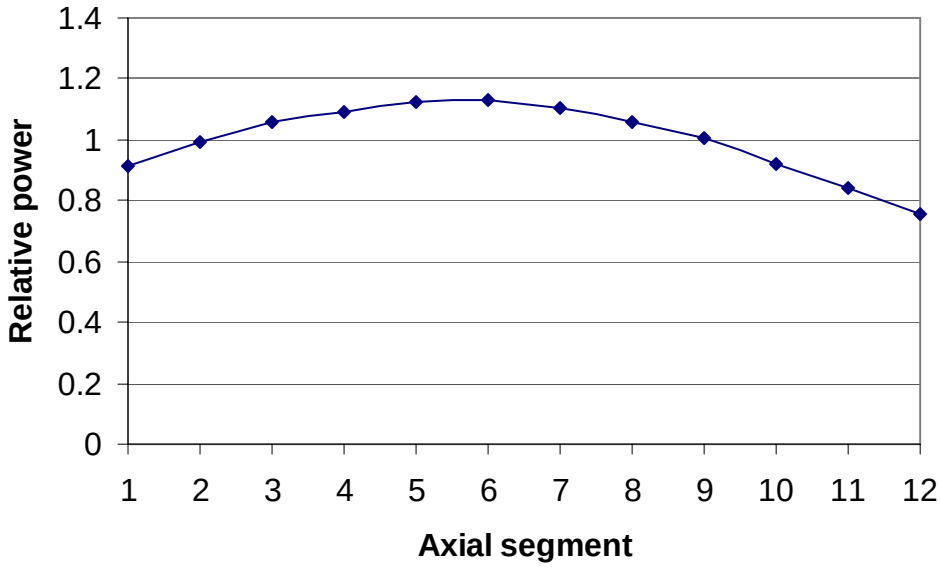

(b)

Figure 19: Ramp power history for the TR-IV Q11/3 rod:
(a) axial peak linear power versus time,
(b) normalized axial power distribution, kept constant during the analysis.

***Results**:*
The axial peak fuel center temperature, the rod free volume pressure and released fission product quantity as a function of time, calculated by SCANAIR, are plotted in figures 20 to 22, respectively. Clad hoop plastic strain and hoop stress for axial segment 6 and radial ring 3 (axial peak power, clad midwall position) are plotted as a function of time in figures 23 and 24, respectively.

***Discussion**:*
As shown in figure 20, the fuel center temperature reaches its peak value T=1500°C at time t=34 s under the ramp, according to the SCANAIR simulation. The fuel-clad gap is completely closed with hard contact at this time; the contact pressure is calculated to be 89.6 MPa at t=34 s. The rod internal pressure increases from about 52 bar at the start of the ramp (conditioning power of 25 kW/m) to a maximum value of 55.7 bar, figure 21. The fission product gas quantity is calculated in units of cm^3 STP (standard temperature pressure). At the end of the ramp, this quantity is about 1.1 cm^3 STP, figure 22. We may estimate the release fraction during the ramp by comparing this quantity with the inventory of gas accumulated in the fuel at the end of the PWR pre-irradiation. We have estimated this inventory to be 146 cm^3 STP, which yields a calculated release fraction of roughly 0.7%, *i.e.* not too far off from the measured value of 0.5%. In this calculation, we have selected the initial fuel porosity pressure to be 6 MPa. These values used for the accumulated fission gas inventory should be calculated carefully with the aid of a steady-state fuel rod computer code, when used as input to SCANAIR.

Clad hoop plastic strain at end of the ramp is calculated to be 0.13%, figure 23, *i.e.* somewhat lower than the measured value of 0.2%, but again, not too afar. The corresponding calculation of clad stress shows a peak hoop stress of 550 MPa during the ramp, figure 24. Radial distributions of plastic hoop strain and hoop stress in the clad are presented in appendix B.

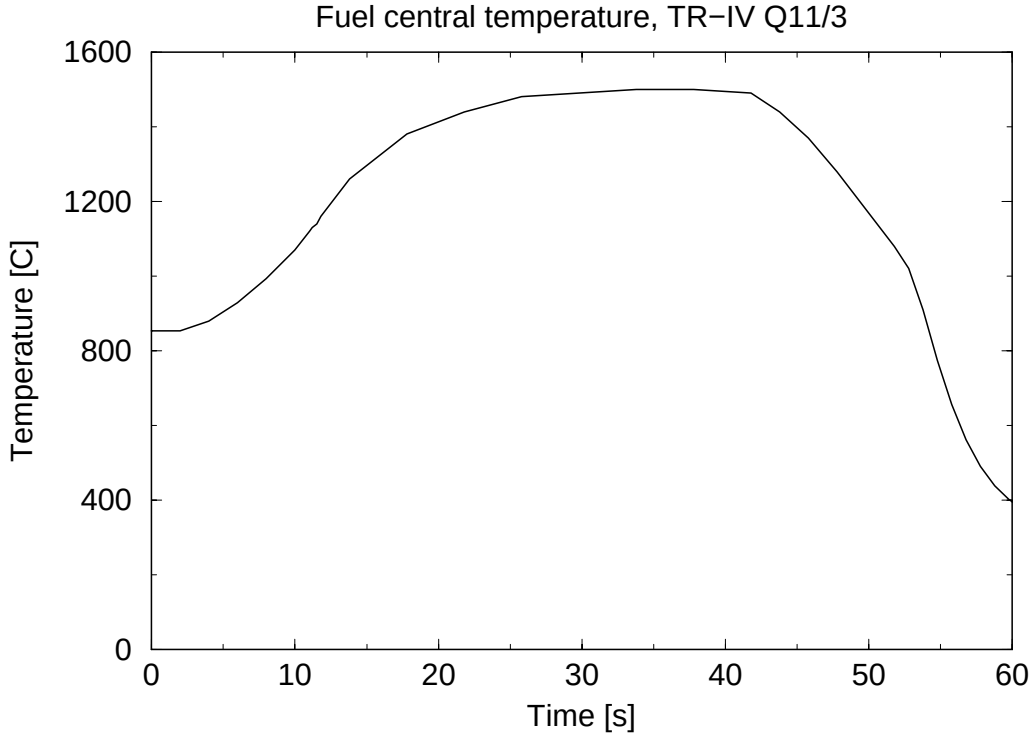

Figure 20: Axial peak fuel center temperature versus time during the power ramp, as calculated by SCANAIR.

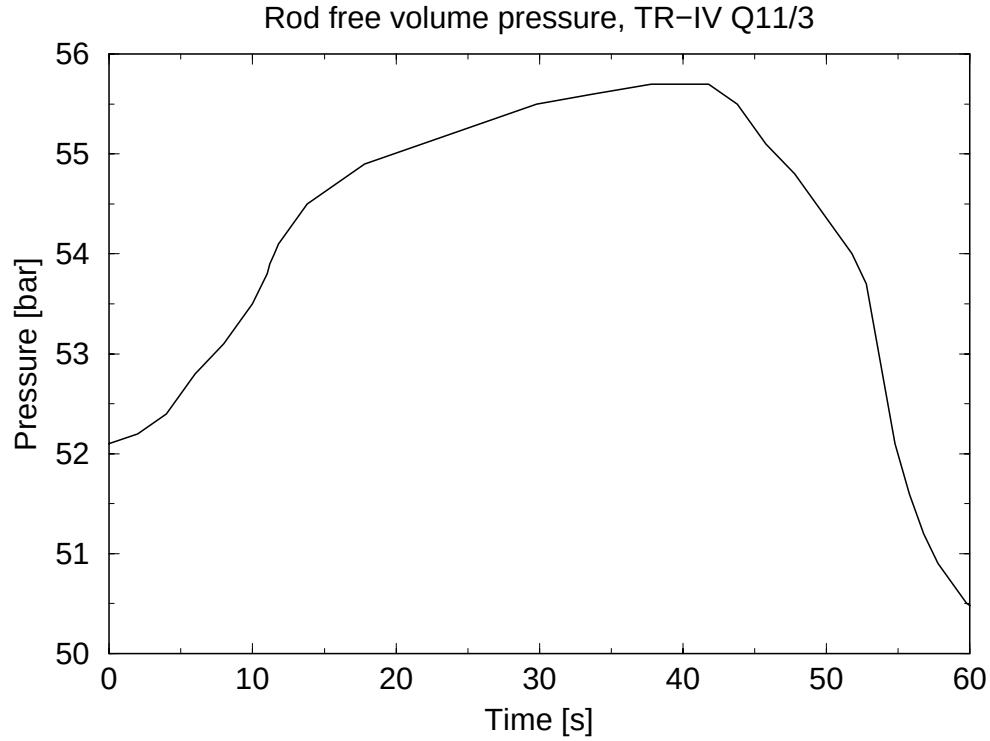

Figure 21: Rod internal pressure versus time, as calculated by SCANAIR.

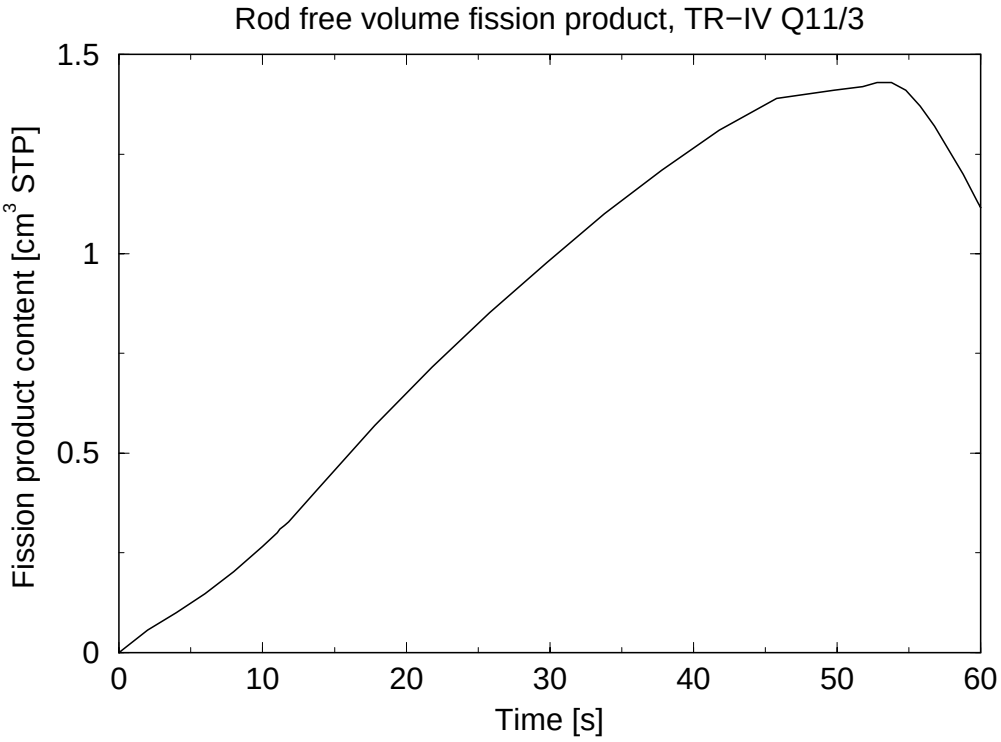

Figure 22: Fission product gas content versus time, as calculated by SCANAIR.

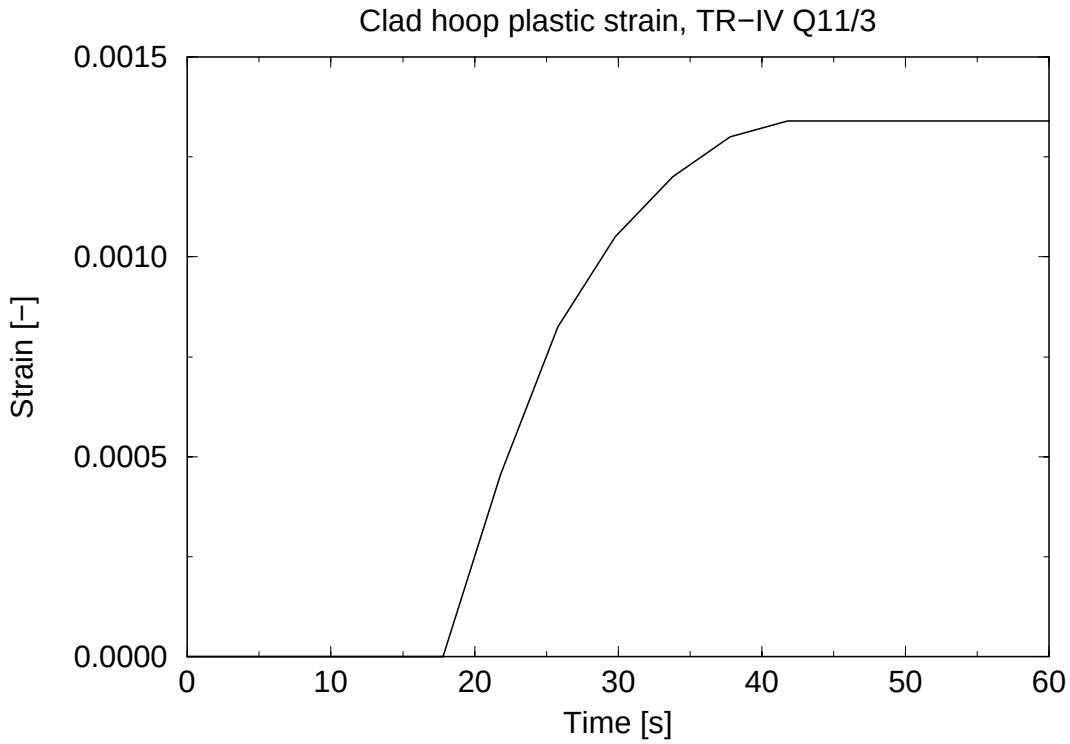

Figure 23: Axial peak clad hoop plastic strain versus time, as calculated by SCANAIR.

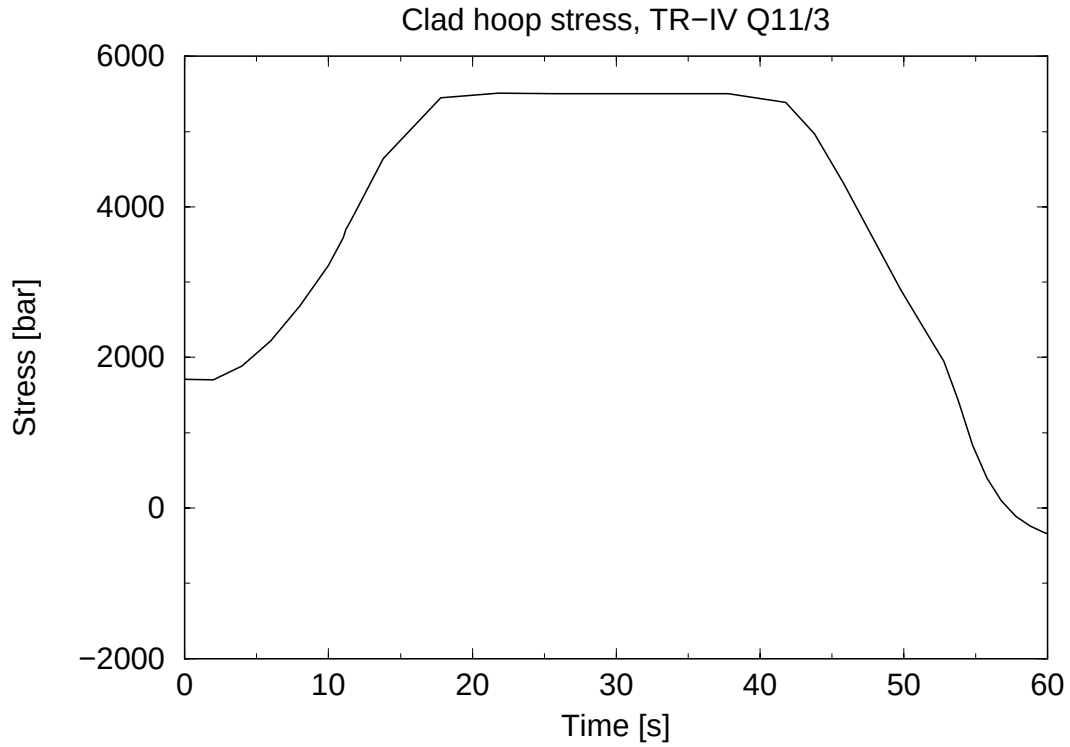

Figure 24: Axial peak clad hoop stress versus time, as calculated by SCANAIR.

5.4 REP Na-2 test case

In this section, we present some results obtained by SCANAIR simulation of an RIA test made on fuel rod REP Na-2 in the CABRI test reactor at the Cadarache research center, Frizonnet *et al.* (1997). REP Na-2 is a PWR fuel rod, which was base-irradiated in the BR3 reactor to an average exposure of 33 MWd/kgU, prior to testing at CABRI. The relatively low burnup, together with a high initial ^{235}U concentration (6.85 wt%) of REP Na-2, allowed a large enthalpy increase during the RIA simulation test; the axial peak radial average enthalpy increased by approximately 200 cal/g. The rod survived the test without clad failure, despite up to 4% hoop plastic strain of the clad during this test, Frizonnet *et al*. (1997).

The SCANAIR input data for REP Na-2 was prepared by IPSN and provided to us for analysis. We refrain from a detailed presentation of input data in this report, since our purpose here is only to test and demonstrate the capability of SCANAIR.

The fuel rod was modeled by dividing it into 20 axial segments for fuel and clad, 20 radial rings for the fuel and 9 radial rings for the clad tube. The oxide layer comprises the two outer rings of the tube.

The transient power history that the rod was subjected to is presented in figure 25a, in the form of peak linear power density (segment 11 from rod bottom) versus time. The constant axial power profile used throughout the transient is shown in figure 25b.

Results:

The calculated axial peak radial average enthalpy versus time is shown in figure 26, and the space-time variation of fuel temperature is depicted in figure 27. In this simulation, the coolant is liquid sodium with inlet temperature 278°C, inlet mass flow rate 0.307 kg/s and a uniform pressure of 0.2 MPa.

The linear power density in this transient reached its peak value of 40.6 MW/m after 80.5 ms; figure 25a. The axial peak radial average fuel enthalpy attained in the transient is 855 J/g, figure 26, and the space-time variation of fuel temperature indicates the expected evolution during fast severe transients. The fuel temperature rises by about 2000°C from t=75 ms to t=200 ms.

Discussion:

We shall not further discuss and evaluate the Na-2 simulation test in the present report. This should be done in a separate study, in which comparisons with other REP-Na series rods should also be made. As mentioned earlier, our purpose here has been to demonstrate SCANAIR's capability to analyze and simulate the fuel rod behavior during postulated reactivity initiated accidents. This capability in general exits with some proviso until a detailed comparison between the tests and calculations is made.

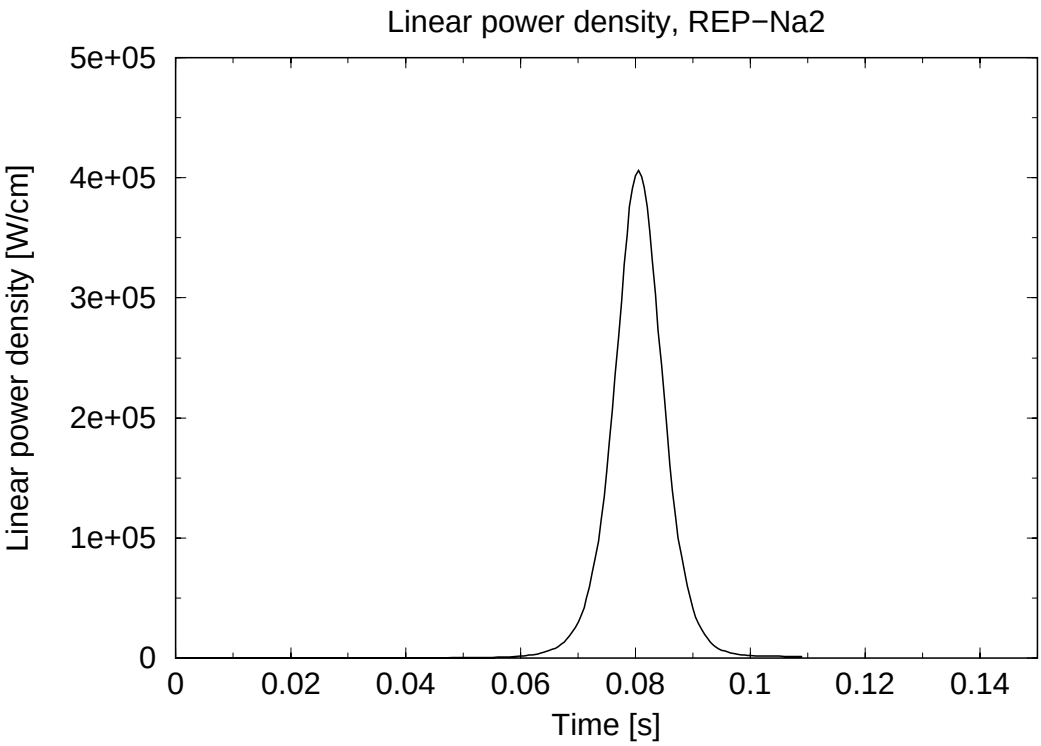

(a)

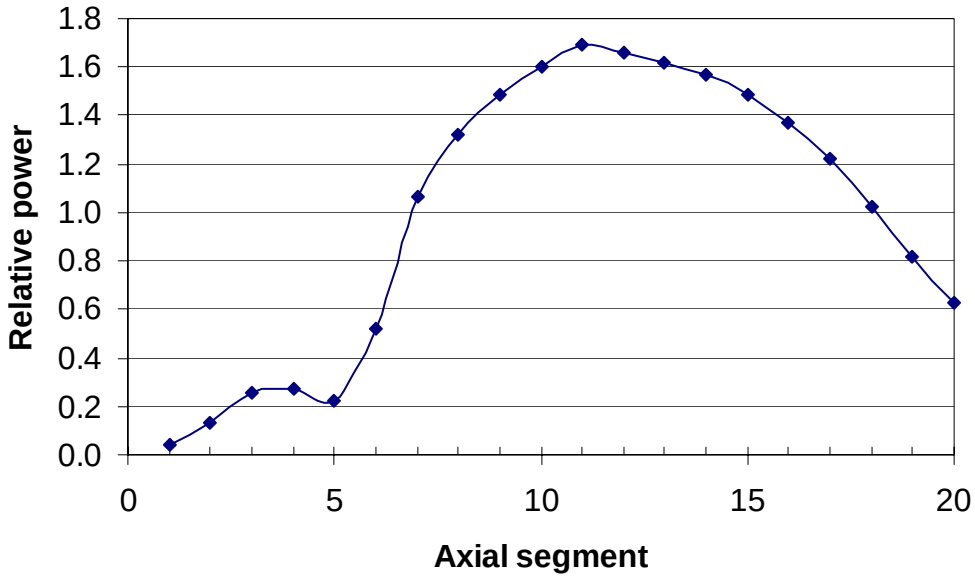

(b)

Figure 25: Transient power history for the REP Na-2 rod:
(a) axial peak linear power versus time (axial segment 11),
(b) normalized axial power distribution, kept constant during the analysis.

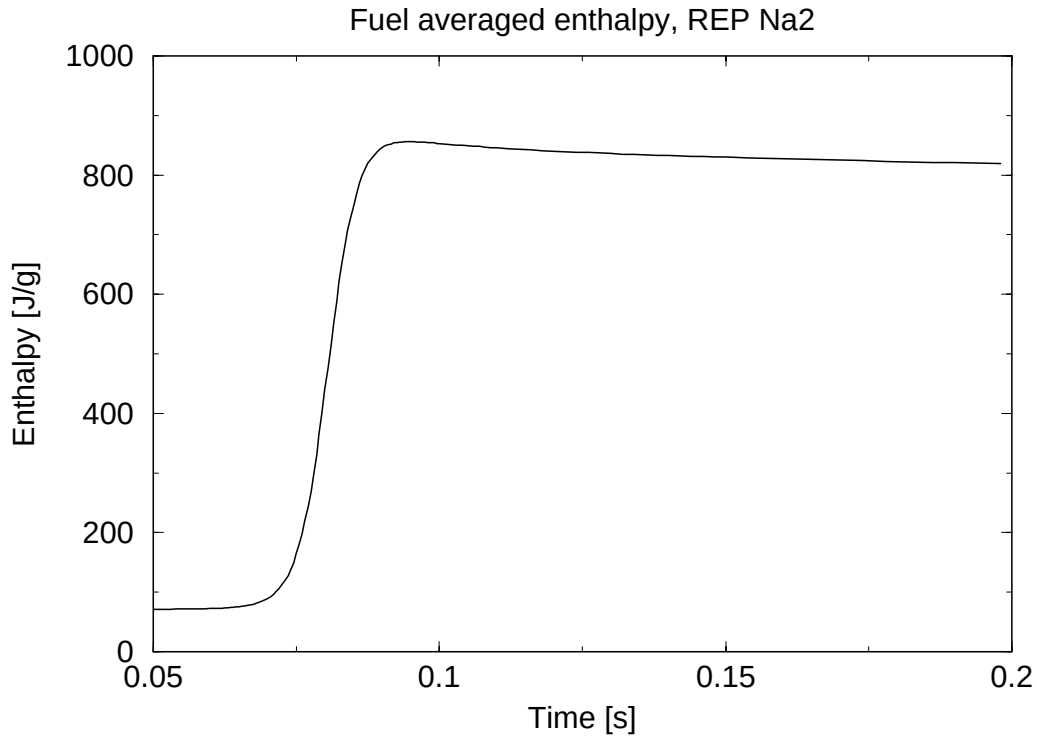

Figure 26: Fuel axial peak radial average enthalpy, as calculated by SCANAIR.

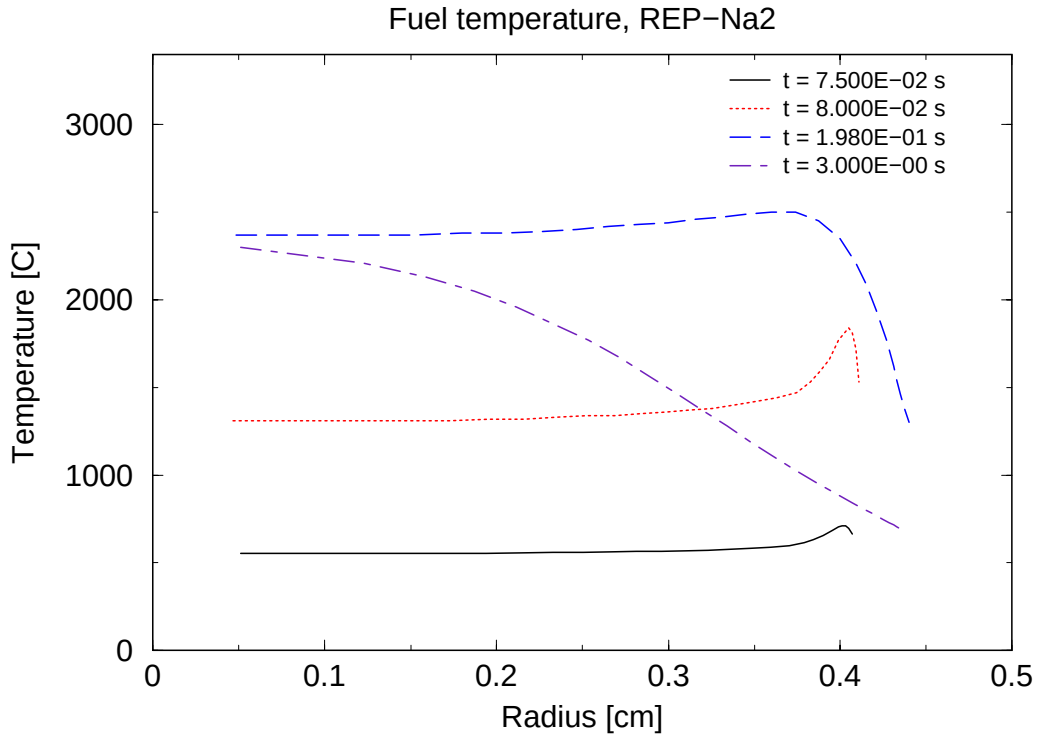

Figure 27: Fuel radial temperature gradient in the peak power axial segment, as calculated by SCANAIR.

6 Concluding remarks

In this report, we have first reviewed the basic theoretical models in the SCANAIR computer code. That is to say, the governing equations for heat transfer, the mechanical response of fuel and clad, and fission gas release behavior are examined, and the range of applicability of the SCANAIR models and their limitations are discussed. We conclude that SCANAIR is designed to study fuel rod thermal-mechanical behavior under fast transients, *i.e*. the kind of transients that are postulated to occur during reactivity initiated accidents (RIA's), and application of SCANAIR to analyze other reactor transients, such as condition II events, is unwarranted.

The code requires an elaborate set of input data at the start of the simulated accident. These data need to be generated by a steady-state fuel rod behavior code. That is, a user of SCANAIR should also have access to a suitable steady-state code in order to define the initial condition of the fuel at start of the RIA, which is postulated to occur at a certain fuel burnup. Moreover, the user also has to supply the transient power history under RIA as input, which requires use of a code for neutronics calculations.

SCANAIR models and correlations include burnup-dependent material parameters. For example, the fuel thermal conductivity relation in SCANAIR is a function of both fuel burnup and fuel porosity. These two parameters evolve spatially across the fuel during irradiation. In particular, the phenomena of porosity increase and grain subdivision at the fuel rim region, which take place in LWR fuel at higher burnups, are catered for in thermal-mechanical computations and in input to the code.

Fuel pellet clad mechanical interaction modeling is somewhat simplistic in SCANAIR. More specifically, SCANAIR does not take into account the friction force between fuel and clad under contact. It assumes that fuel and clad are bond together as a single solid cylinder during contact, rather than two dynamically interacting bodies. The consequence of this simplification on the mechanical response of the clad is not explored here, but it is an aspect that more attention should be paid upon in a future study. To this end, we note that models used for the inelastic deformation behavior of Zircaloy clad materials are rather primitive, since they neglect both anisotropy and viscoplastic effects.

Another simplification in the SCANAIR thermal models concerns gas mixing in the pellet-clad gap. SCANAIR assumes that gases that are released during the transient mix instantaneously and completely with the existing gas in the gap and in the rod plena. We know from both experimental and theoretical studies that there is a delay time for gas mixing. The feedback of this phenomenon on fuel temperature should also be explored in a future study.

We have performed a number of computations with SCANAIR. These include, i) prediction of thermal-mechanical behavior of a high-burnup fuel rod during a hypothetical "mild" RIA, ii) a simulation of a power ramp experiment made at the Studsvik R2 reactor and iii) a calculation of a severe RIA test made in the CABRI test reactor. We also have compared some of the results computed by SCANAIR with those of an independent in-house code. The outcome of our analyses has been agreeable.

Finally, we should mention that we have not subjected SCANAIR to an extensive testing and benchmarking against experimental data, nor have we made a wide-range parametric study to locate the pitfalls of the code, when analyzing the complex behavior of a highly irradiated fuel rod under RIA. Nevertheless, our limited study with SCANAIR has been encouraging. We believe that SCANAIR is a state of the art computer program for predicting the thermal-mechanical behavior of a fuel rod during a postulated RIA, but that models used within the program need further verification and calibration with experimental data.

Acknowledgements

We would like to express our gratitude to Francois Lamare of IPSN for assistance with the installation of SCANAIR and many E-mail communications regarding input data and transfer of files. We are also grateful to Ingrid Töcksberg of SKI and David Schrire of the Studsvik Nuclear concerning information on the TRANSRAMP-IV tests and measurements. We also thank our colleague Tero Manngård for his interest on the subject during the course of the work. The work was supported by the Swedish Nuclear Power Inspectorate under Award 14.6-010185/01088.

7 References

Balourdet, M., Bernaudat, C., Basini, V.and Hourdequin, N., *The PROMETRA program: assessment of mechanical properties of Zircaloy 4 cladding during an RIA*, SMiRT-15 conference, Seoul, Korea, August 1999.

Chandrasekhar, S., *Stochastic problems in physics and astronomy*, Reviews of Modern Physics, vol. 15, pp. 1-89, 1943.

Constantinescu, A., Dragon, M. and Kichenin, J., *Programming engineering applications using the object oriented FEM code CASTEM 2000*, SIAM Workshop on Object Oriented Methods for Interoperable Scientific and Engineering Computing (OO98), IBM Research, Yorktown, New York, 1998.

Delobelle, P., Robinet, P., Bouffioux, P., Geyer, P. and Le Pichon, I., *A unified model to describe the anisotropic viscoplastic behaviour of Zircaloy-4 cladding tubes*, Zirconium in the Nuclear Industry: 11th International Symposium, eds. E.R. Bradley and G.P. Sabol, American Society for Testing and Materials, ASTM STP 1295, March 1996.

Djurle, S., *Final report of the TRANS-RAMP IV project*, Studsvik Report STUDSVIK/STTRIV-25, Draft No 1, Studsvik, Sweden, March 1993.

Federici, E., Lamare, F., Bessiron, V. and Papin, J., *Status of development of the SCANAIR code for the description of fuel behavior under reactivity initiated accidents*, ANS Light Water Reactor Fuel Conference, Park City, Utah, April 10-13, 2000a.

Federici, E., Lamare, F., Bessiron, V., Lemoine, F. and Papin, J., *The SCANAIR code version 3.2: Application to the interpretation of the NSRR TK1 test*, The 24th NSRR technical review meeting, Tokyo, Japan, November 13-14, 2000b.

Frizonnet, J-M., Breton, J-P., Rigat, H. and Papin, J., *The main outcomes from interpretation of the CABRI REP-Na experiments for RIA study*, International Topical Meeting on Light Water Reactor Fuel Performance, Portland, Oregon, March 2-6, 1997.

Fuketa, T., Sasajima, H., Tsuchiuchi, Y., Mori, Y., Nakamura, T. and Ishijima, K., *NSRR/RIA experiments with high burnup PWR fuels*, International Topical Meeting on Light Water Reactor Fuel Performance, Portland, Oregon, March 2-6, 1997.

Glasstone, S. and Sesonske, A., *Nuclear Reactor Engineering, 3rd Edition*, Table A.6, Krieger Publishing Company, Malabar, Florida, 1991.

Hagrman, D. L., and Reymann, G. A., *MATPRO-version 11, A handbook of material properties for use in analysis of light water reactor fuel behavior*, US NRC Report NUREG/CR-0497, Washington DC, 1979.

Haste, T.J., *A review of axial gas communication in oxide fuel rods*, Paper presented at the Enlarged Halden Group Meeting on Fuel Performance Experiments and Analysis, Loen, Norway, May 8-13, 1988.

Jacq, F., *SIGAL 98: Reference manual, revision 2*, Note technique IPSN/DRS/SEMAR 98/48, Cadarache, France, 1998.

Lamare, F. and Latché, J-C., *SCANAIR: A computer program for reactivity initiated accidents in LWRs*, IPSN Report DRS/SEMAR 95/01, Cadarache, France, 1995.

Lamare, F., *The SCANAIR code version 2.3:Rreference documentation*, IPSN Report DRS/SEMAR 98/107, Cadarache, France, 1998.

Lamare, F., *The SCANAIR code version 3.2:Rreference documentation*, IPSN Report DRS/SEMAR 01/37, Cadarache, France, 2001.

Landau, L.D. and Lifshitz, E.M., *Theory of elasticity, 2nd edition*, Pergamon Press, Oxford, UK, 1970.

Latché, J.C., Lamare, F. and Cranga, M., *Computing reactivity initiated accidents in PWR's*, SMiRT-13 conference, Porto Alegre, Brazil, August 13-18, 1995.

Lemoine, F. and Balourdet, M., *RIA-related analytical studies and separate effect tests*, International Topical Meeting on Light Water Reactor Fuel Performance, Portland, Oregon, March 2-6, 1997.

Massih, A.R. and Jernkvist, L.O., *STRUCTUS: Theory and modelling bases*, Quantum Technologies Technical Report TR 01-001, 2001.

Matthews, J.R., and Wood, M.H., *A simple operational gas release and swelling model: II grain boundary gas*, Journal of Nuclear Materials, vol. 91, pp. 241-256, 1980.

Olander, D. R., *Fundamental Aspects of Reactor Fuel Element*, U.S. Department of Commerce Document TID-26711-P1, Springfield, Virginia, 1976.

Papin, J., Balourdet, M., Lemoine, F., Lamare, F., Frizonnet, J-M. and Schmitz, F., *French studies on high-burnup fuel transient behavior under RIA conditions*, Nuclear Safety, vol. 37, pp. 289-237, 1996.

Papin, J, Rigat, H., Lamare F. and Cazalis B., *The SCANAIR code for the description of PWR fuel rod behavior under RIA: Validation on experiments and extrapolation to reactor conditions*, International Topical Meeting on Light Water Reactor Fuel Performance, Portland, Oregon, March 2-6, 1997.

Pontoizeau, B., *Introduction of an isotropic strain hardening plasticity model in the SCANAIR code*, IPSN Report DRS/SEMAR 98/80, Cadarache, France, 1998.

Sontheimer, F., Dewes, P., Manzel, R. and Stehle, H., *Release of the volatile fission products Xe, Kr, Cs from PWR fuel under steady and transient conditions up to high burnup*, IAEA Technical Committee on fuel rod internal chemistry and fission product behaviour, Karlsruhe, 1985.

Wood, M.H., Matthews, J.R. and Matthews, H.R., *Comparison of experiment and NEFIG model calculations of transient fission gas behavior*, Journal of Nuclear Materials, vol. 87, pp. 167-174, 1979.

Appendix A: REP4 test case

Some of the results of the test transient case discussed in section 5.1 are presented in this appendix. The considered fuel rod is a hypothetical 17×17-array PWR rod, which has been pre-irradiated for 4 years. The segment of the rod subjected to a transient simulation had an average burnup of 7.44 atom%, corresponding to an exposure of about 69.5 MWd/kgU. The segment comprised a fuel volume of 30.8 cm^3, with a total mass of 309 g.

The pre-irradiation calculation was made with the code TOSURA at IPSN. Some of the output data from that code were used as input to SCANAIR, and are listed in tables A1 and A2. Fuel and clad materials are UO_2 and Zircaloy-4, respectively.

Table A1: Fuel rod dimensions at the end of pre-irradiation

Axial elevation	Fuel radius	Clad inner radius	Clad outer radius	Oxide layer thickness
mm	mm	mm	mm	mm
189.2	4.13679	4.13831	4.73850	0.046
378.4	4.13923	4.14116	4.75350	0.075
567.6	4.14942	4.15117	4.75150	0.050

Table A2: Fuel rod dimensions and properties at the beginning of transient

Plenum volume, lower	mm^3	361
Plenum volume, upper	mm^3	1034
Gas, helium	mm^3 STP	3918
Grain radius, center	μm	5.65
Grain radius, rim	μm	0.1

The relative power (radial form factor), the plutonium-concentration, and burnup across the fuel radius for axial segment 7 (the peak power axial position) are plotted in figures A1 to A3, respectively. The Pu-concentration is defined as follows:

$$Pu\_C = \frac{Number\ of\ Pu\ atoms}{Number\ of\ Pu\ and\ U\ atoms} \qquad (A.1)$$

***Results**:*

The transient power history for the case under study is shown in figure 10. The results of the SCANAIR computation for the axial segment 7 at different instants during the transient are given in the following figures. Radial variations of fuel and clad temperatures are plotted in figures A4 and A5, respectively, whereas figure A6 shows the coolant bulk temperature. Heat transfer coefficients from clad to coolant and from pellet to clad are shown in figures A7 and A8, respectively. Fuel swelling strain is depicted in figure A9. The data for the clad hoop plastic strain, hoop stress and the plastic strain energy density are displayed in figures A10 to A12.

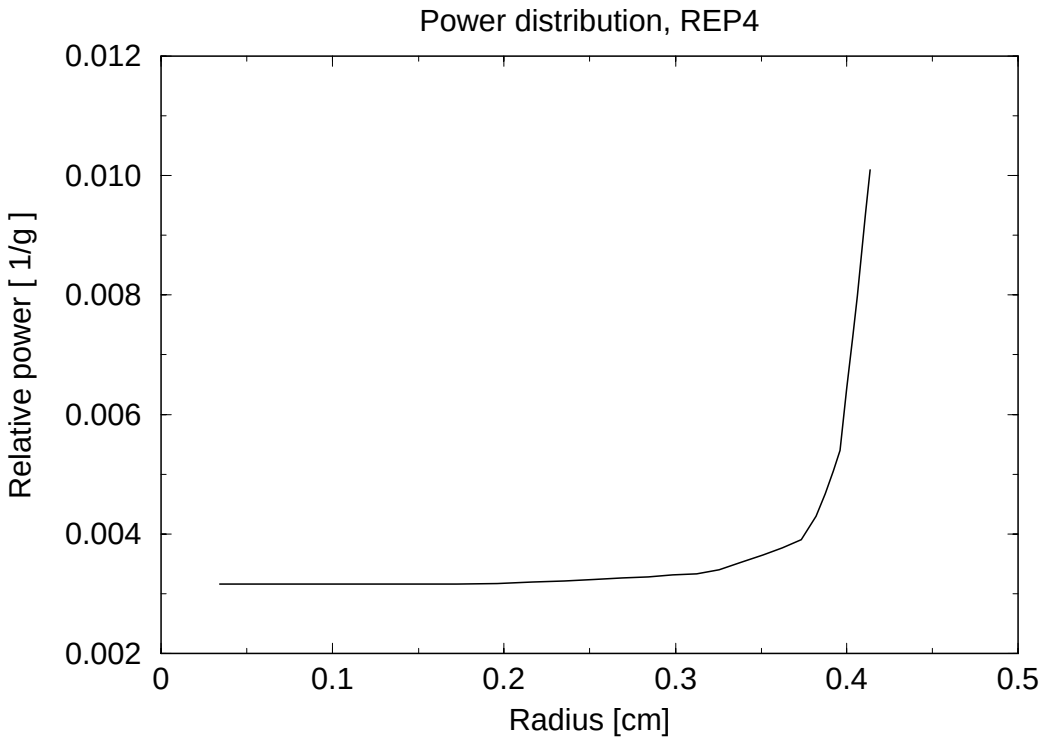

Figure A1: Relative power across fuel at the end of pre-irradiation, as calculated by TOSURA. The power profile was applied in the transient analysis with SCANAIR.

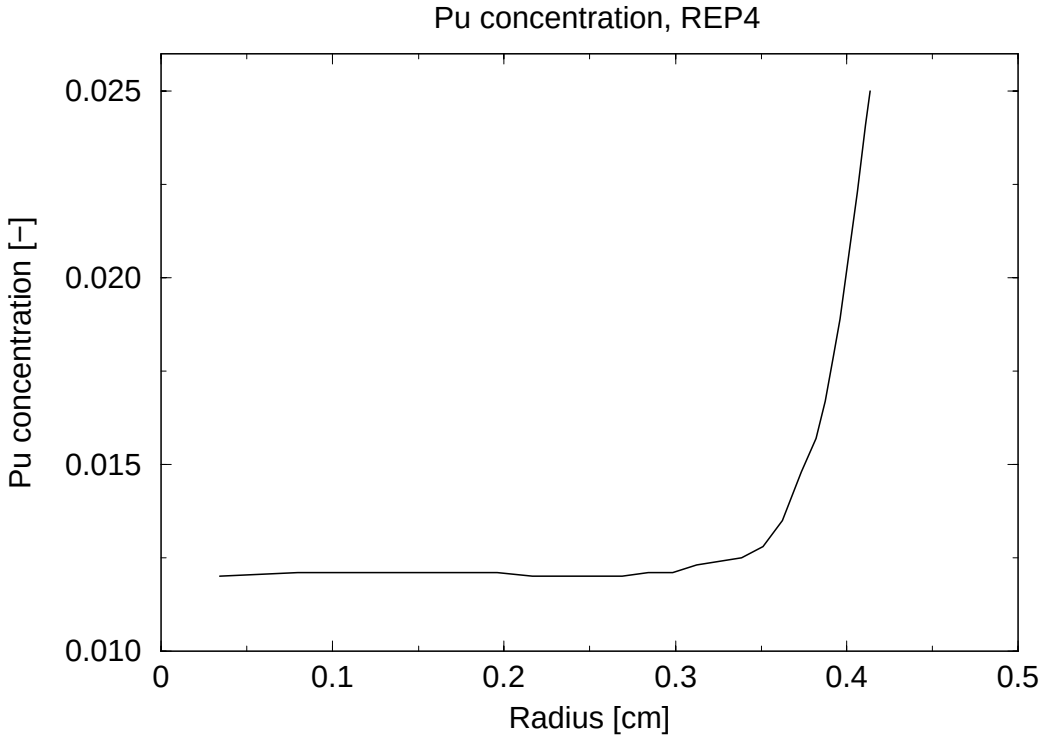

Figure A2: Plutonium concentration across fuel at the end of pre-irradiation, as calculated with TOSURA.

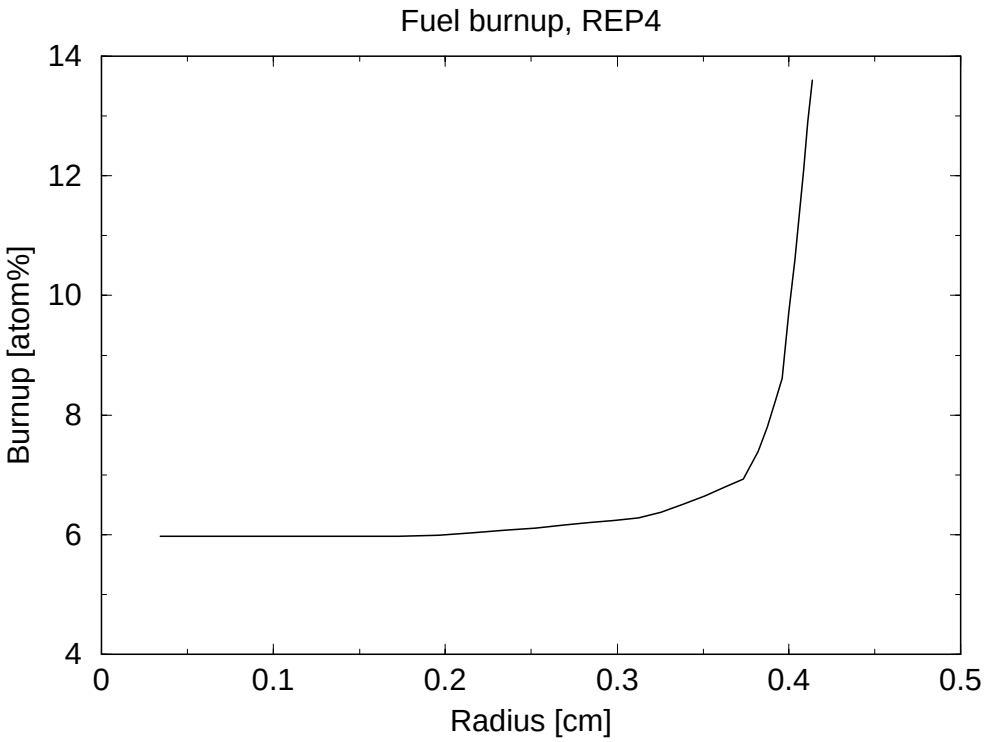

Figure A3: Burnup across fuel at the end of pre-irradiation, as calculated with TOSURA

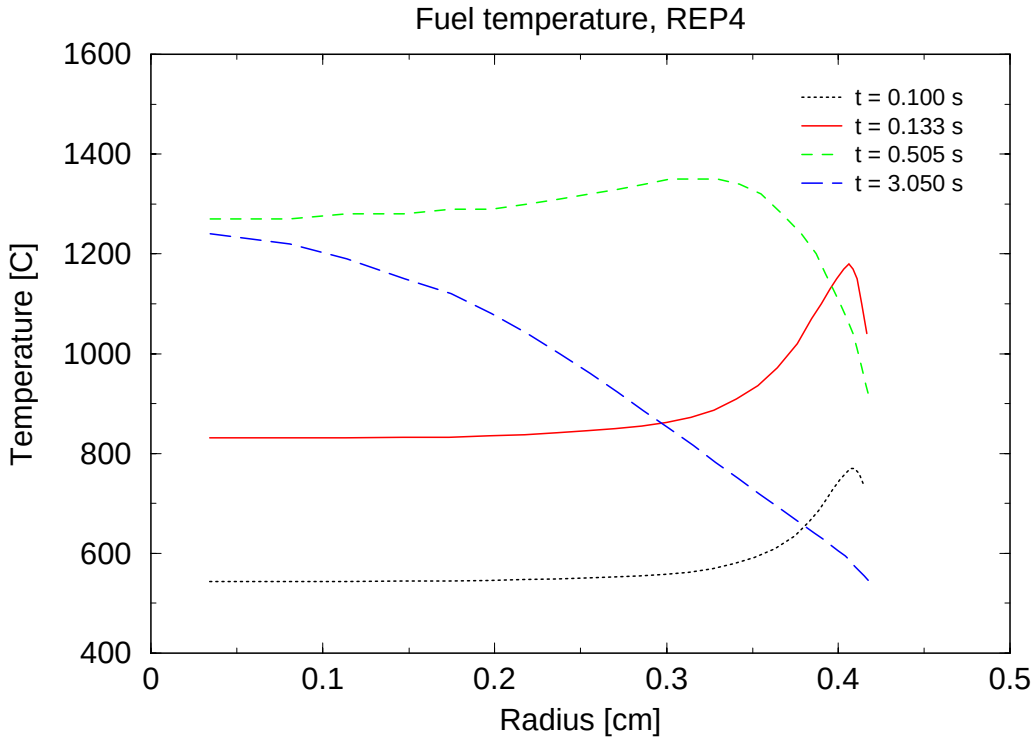

Figure A4: Fuel temperature variation in space and time during the transient, as calculated by SCANAIR.

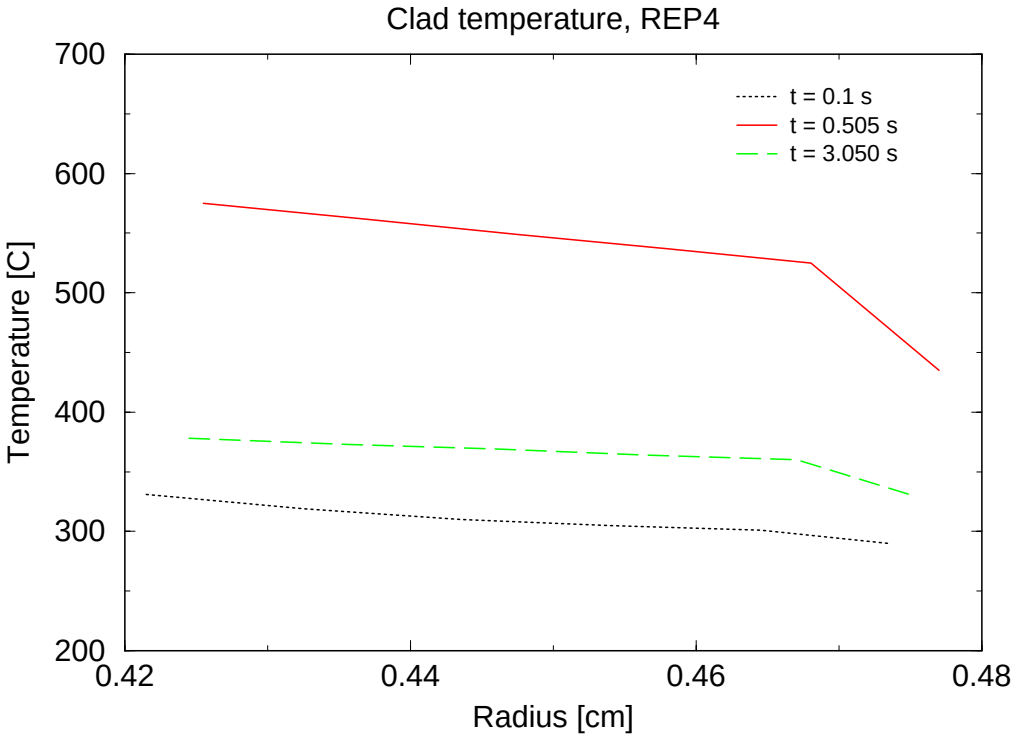

Figure A5: Calculated clad temperature variation in space and time during the transient.

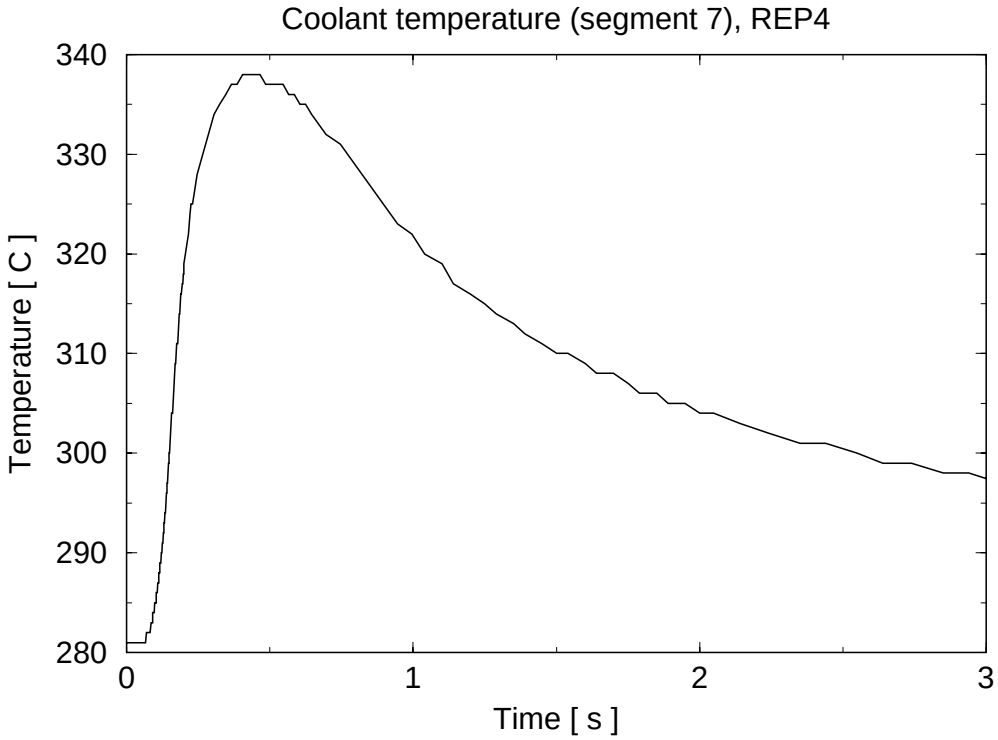

Figure A6: Calculated coolant temperature at the peak power axial segment.

***Discussion**:*

In figure A4, we observe a shift of peak temperature from the surface of the fuel to its center from time *t*=0.1 s to *t*=0.5 s; a characteristic of rapid power excursions in nuclear fuel. Figure A5 displays the corresponding values for the clad temperature. The rise and fall of clad temperature during the transient, *i.e.*, from *t*=0.1 to *t*=0.5 s and then to *t*=3 s, can be seen from this figure. The knees in the curves indicate the transition from Zircaloy to the clad outer oxide (ZrO_2) layer.

The sodium bulk temperature in the coolant channel at the peak power axial segment increases by approximately 60°C, as shown in figure A6. The clad to coolant heat transfer remains very efficient throughout the entire transient, as shown in figure A7.

The pellet to clad heat transfer coefficient is shown in figure A8. The sudden decrease in heat transfer is due to the rapid release of accumulated fission gas during the early part of the transient. To this end, it should be recalled that complete and instantaneous mixing of released fission gas is assumed in SCANAIR. If the delay in fission gas mixing were considered by use of a more realistic model, the thermal insulation effect displayed in figure A8 would be even stronger.

The fuel swelling strain due to fission products at two different time points during the transients, *i.e.* at *t*=0.5 s and *t*=3 s, shows a strong space-time dependence; figure A9. Early during the transient, the fuel rim region swells. Then, as shown for *t*=3 s, the swelling shifts toward the center. The swelling is zero in the central part of the fuel, since the fission product gases have already been released in that region. The small negative values for the swelling strain seen in figure A9 are believed to be artifacts of numerical noise (instability) of the code.

The clad hoop plastic strain and hoop stress decrease and increase, respectively, across the clad wall thickness; figure A10 and A11. An average hoop plastic strain of about 0.6 % is calculated at *t*=3 s. The knees seen in these figures are again due to the transition to the oxide layer, which does not sustain any stress and plastic deformation under loading, according to the SCANAIR models. The plastic strain energy density shown in figure A12 is fairly constant across the clad tube wall. At *t*= 0.5 and *t*=3 s, the calculated plastic strain energy density is around 4 J/cm^3.

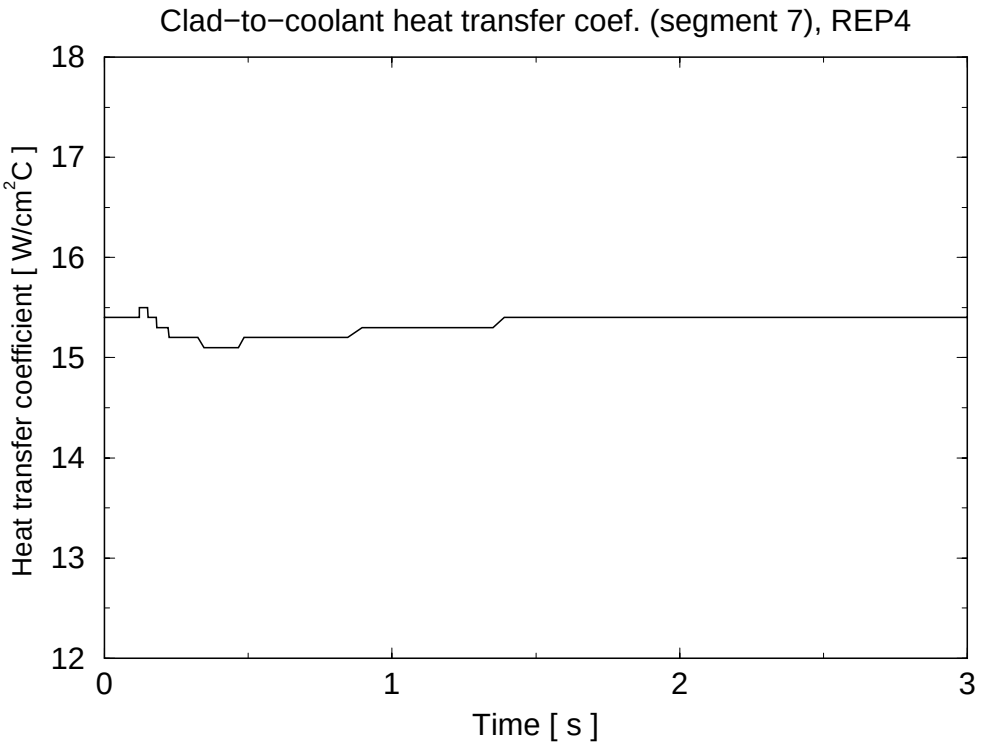

Figure A7: Calculated clad to coolant heat transfer coefficient at the peak power axial position.

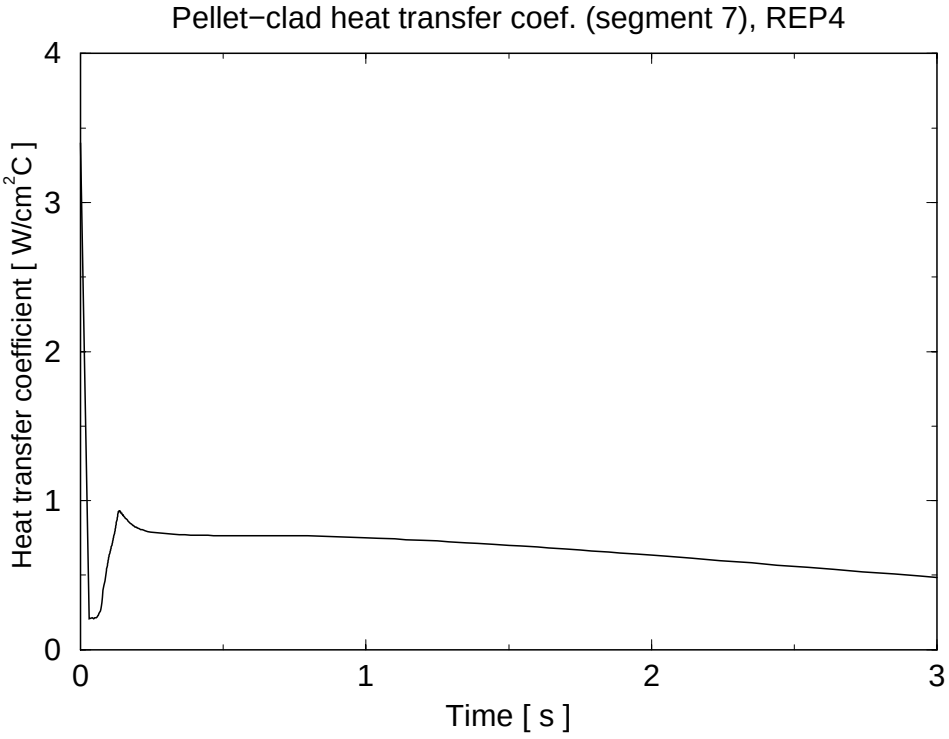

Figure A8: Calculated fuel pellet to clad heat transfer coefficient at the peak power axial position.

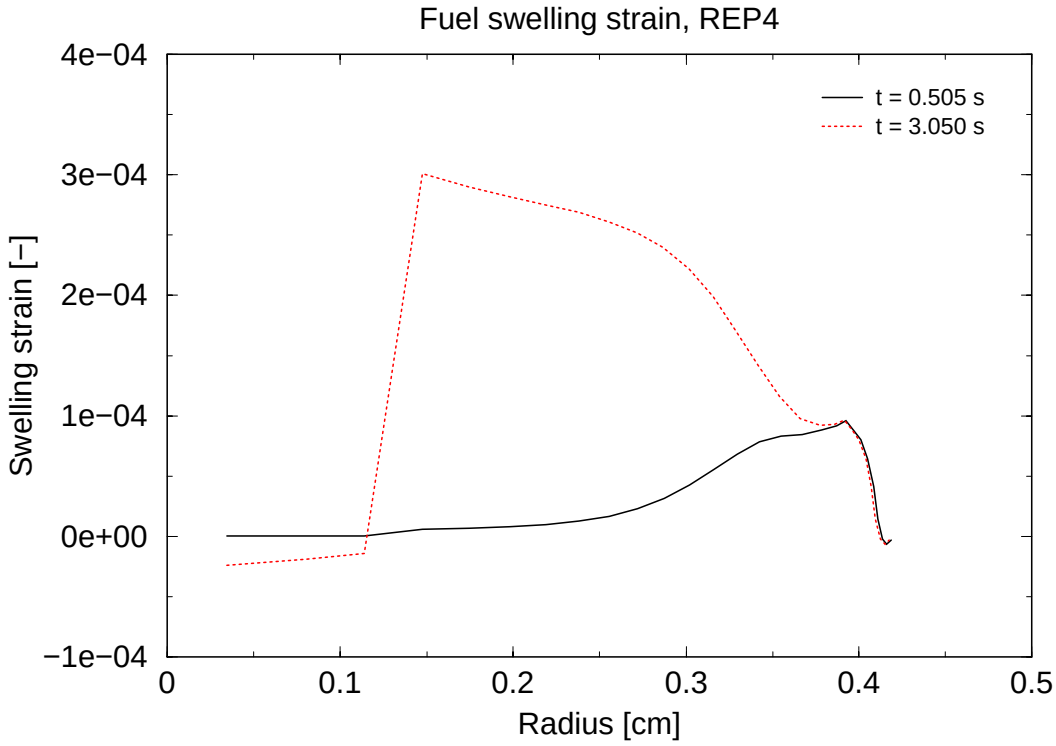

Figure A9: Calculated swelling strain across fuel due to the expansion of fission gas bubbles at different times during the transient.

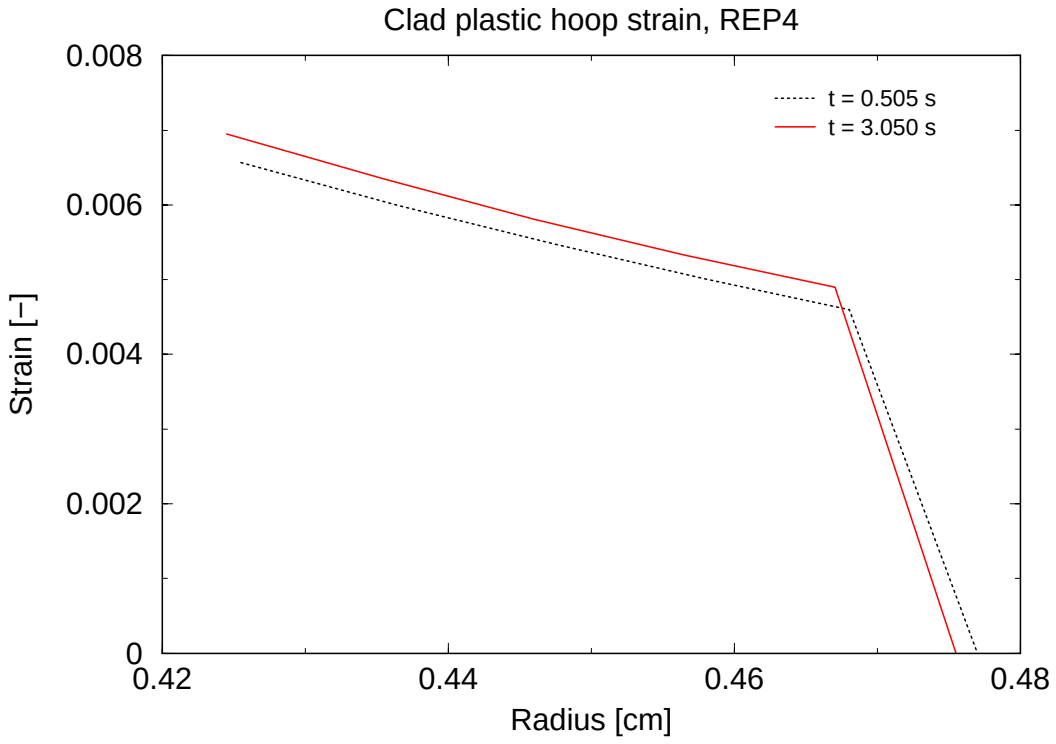

Figure A10: Calculated hoop plastic strain across clad wall at different times during the transient. The outermost layer with zero plastic strain corresponds to the oxide.

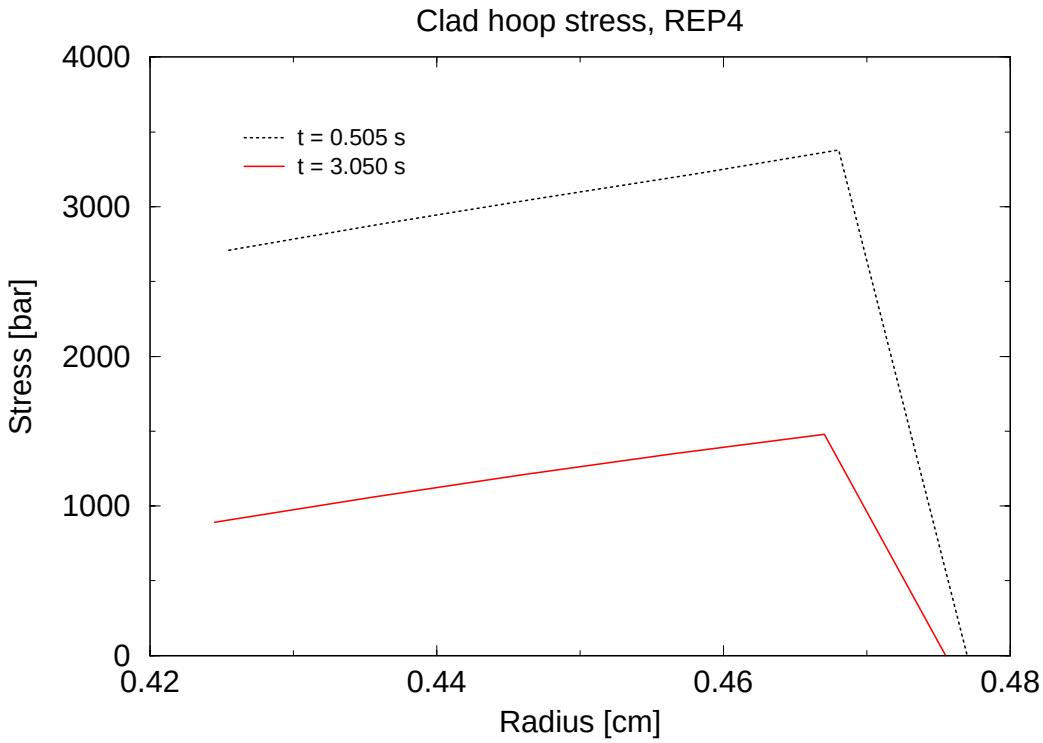

Figure A11: Calculated hoop stress across clad wall at different times during the transient.

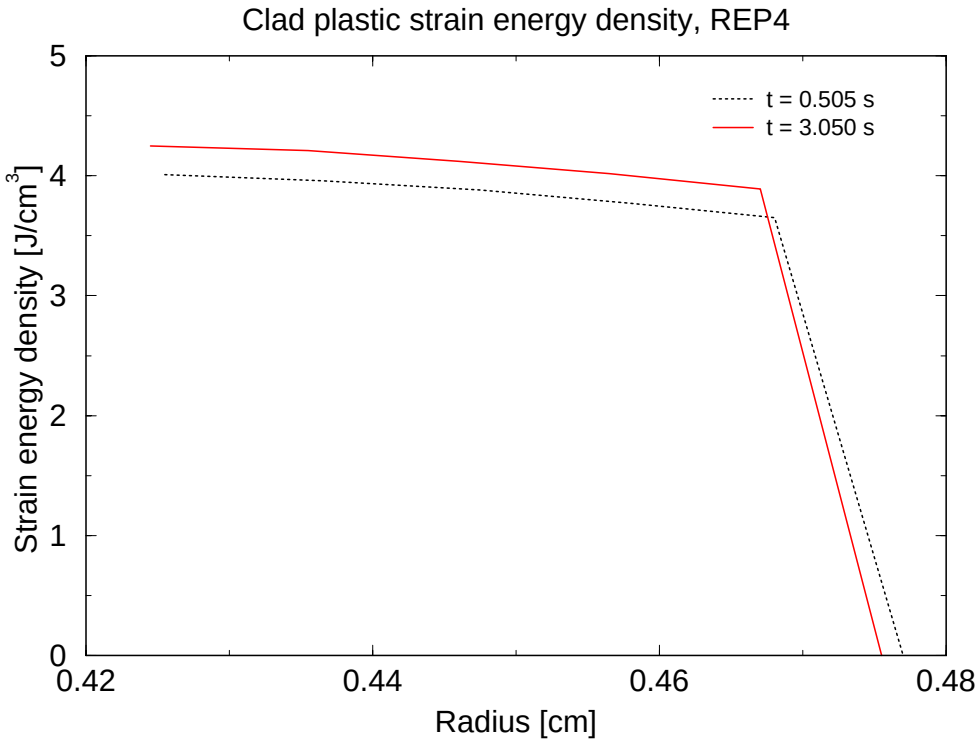

Figure A12: Calculated plastic strain energy density across clad wall at different times during the transient.

Appendix B: TRANSRAMP-IV test case

Some of the results of the evaluation of the TR-IV rod Q11/3, discussed in section 5.3, are presented in this appendix. The rod is a 17×17-array PWR rod, which has been pre-irradiated for 2 years in the French GRAVELINES 3 reactor. The segment of the rod that is subjected to ramp simulation had an average exposure of about 29 MWd/kgU.

The pre-irradiation data needed for the SCANAIR input are obtained by hand-calculation, using the data reported in the TR-IV final report, Djurle (1993), and our technical judgment. Some of these data are listed in tables B1 and B2. Fuel and clad materials are UO_2 and Zircaloy-4, respectively.

Table B1: Fuel rod dimensions at the end of pre-irradiation

Axial elevation	Fuel radius	Clad inner radius	Clad outer radius	Oxide layer thickness
mm	mm	mm	mm	mm
115.33	4.1414	4.1435	4.7135	0.010
230.67	4.1415	4.1435	4.7135	0.010
346	4.1425	4.1435	4.7135	0.010

Table B2: Fuel rod dimensions and properties at the beginning of ramp

Plenum volume, lower	mm^3	0
Plenum volume, upper	mm^3	2380
Gas, helium	mm^3 STP	54150
Grain radius, center	μm	6.34
Grain radius, rim	μm	6.34

The ramp power history for the case under study is shown in figure 15. The results of the SCANAIR computations for the radial variation of clad hoop plastic strain and clad hoop stress for axial segment 6, where load is at maximum, are presented in figures B1 and B2, respectively. The clad hoop plastic strains shown in figure B1 are at end of ramp, while B2 shows the clad hoop stress at t =30 s under the ramp, where the stress level reaches its highest value. The knees in the plots indicate the transition to the oxide layer at the outer rim of the cladding tube, which according to SCANAIR does not bear any stress and does not deform plastically.

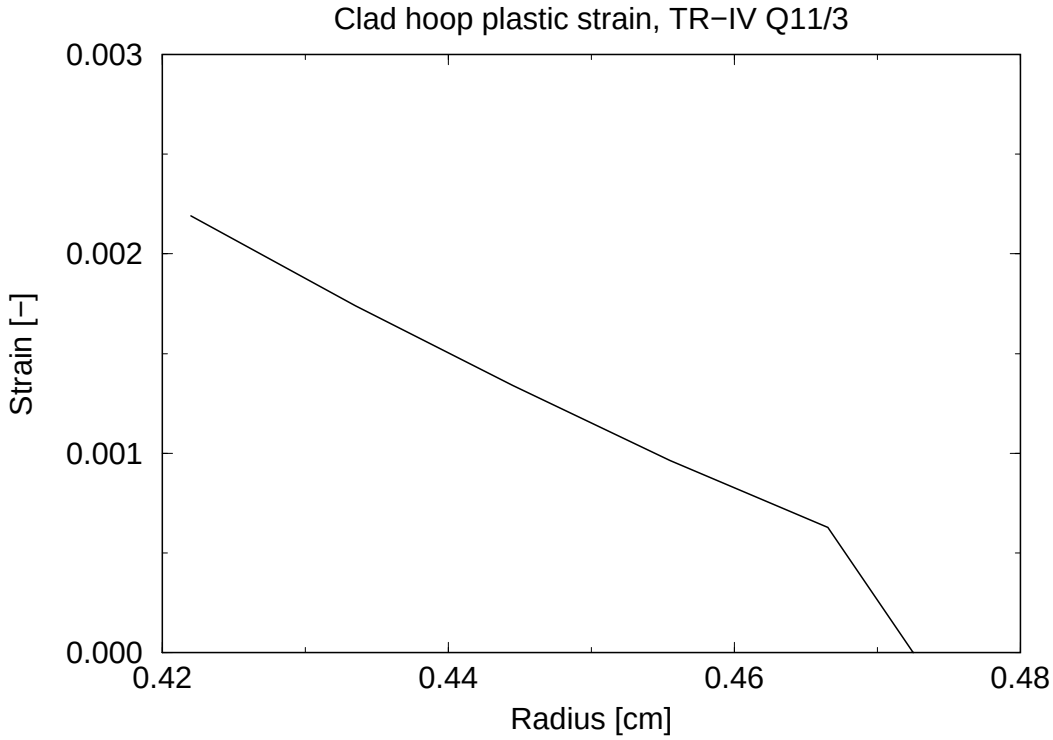

Figure B1: Calculated axial peak radial profile of clad hoop plastic strain at end of ramp.

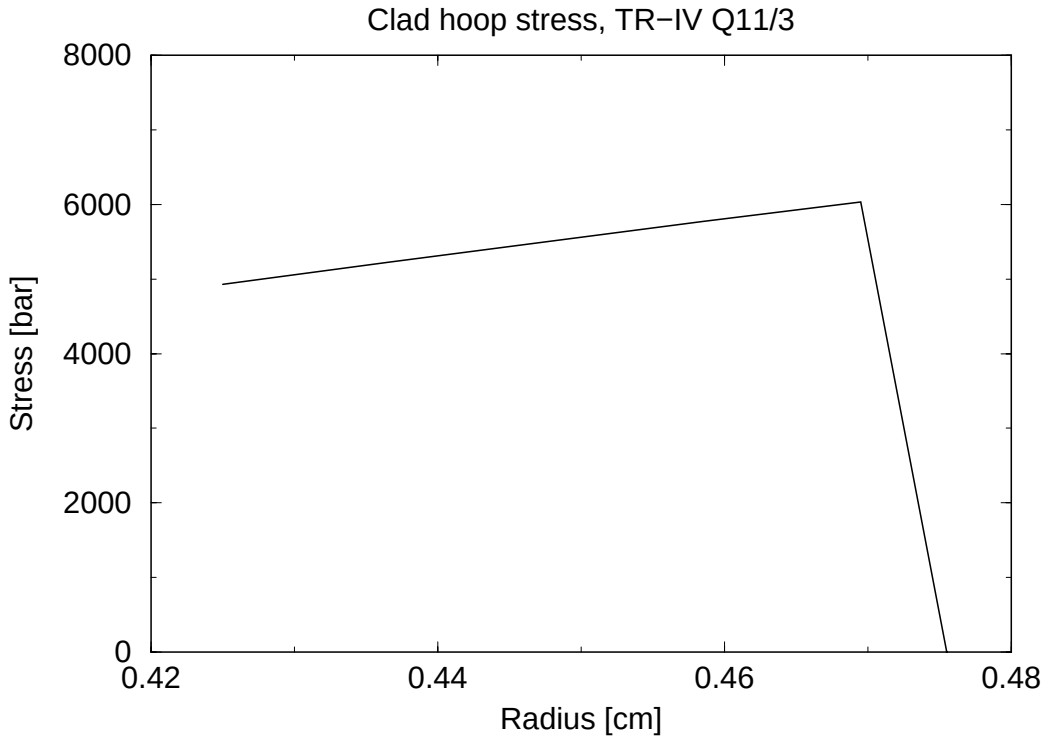

Figure B2: Calculated axial peak radial profile of clad hoop stress at maximum under ramp.